Developmental Biology 508 (2024) 123–137

Contents lists available at ScienceDirect

Developmental Biology

journal homepage: www.elsevier.com/locate/developmentalbiology

microRNA-1 regulates sea urchin skeletogenesis by directly targeting skeletogenic genes and modulating components of signaling pathways

Nina Faye Sampilo [a,b], Jia L. Song [a,*]

[a] Department of Biological Sciences, University of Delaware, Newark, DE, 19716, USA
[b] Invitae - Metropark (formerly Genosity), Iselin, NJ, 08830, USA

ARTICLE INFO

Keywords:
Sea urchin
Skeletogenesis
Post-transcriptional regulation

ABSTRACT

microRNAs are evolutionarily conserved non-coding RNAs that direct post-transcriptional regulation of target transcripts. In vertebrates, microRNA-1 (miR-1) is expressed in muscle and has been found to play critical regulatory roles in vertebrate angiogenesis, a process that has been proposed to be analogous to sea urchin skeletogenesis. Results indicate that both miR-1 inhibitor and miR-1 mimic-injected larvae have significantly less F-actin enriched circumpharyngeal muscle fibers and fewer gut contractions. In addition, miR-1 regulates the positioning of skeletogenic primary mesenchyme cells (PMCs) and skeletogenesis of the sea urchin embryo. Interestingly, the gain-of-function of miR-1 leads to more severe PMC patterning and skeletal branching defects than its loss-of-function. The results suggest that miR-1 directly suppresses *Ets1/2, Tbr,* and *VegfR7* of the skeletogenic gene regulatory network, and *Nodal,* and *Wnt1* signaling components. This study identifies potential targets of miR-1 that impacts skeletogenesis and muscle formation and contributes to a deeper understanding of miR-1's function during development.

1. Introduction

microRNA-1 (miR-1) is among the most evolutionarily conserved microRNAs (Nguyen and Frasch, 2006). miR-1 is classified as a myomiR because of its enriched expression in the muscle of vertebrates and its important role in myogenesis, angiogenesis, and vascularization (Mansfield et al., 2004; McCarthy, 2011; Sokol and Ambros, 2005; Wienholds et al., 2005; Zhao et al., 2005). In mice, miR-1 loss-of-function and gain-of-function led to aberrant heart morphogenesis, myogenic differentiation, and cell proliferation (Chen et al., 2006; Zhao et al., 2005, 2007). It was proposed that vertebrate miR-1 finetunes the levels of transcripts encoding proteins that are essential for heart function, rather than suppressing non-muscle genes in other tissues (Mishima et al., 2007). Extensive studies have demonstrated miR-1's role in blocking cardiomyocyte proliferation and skeletal muscle differentiation in both vertebrates and invertebrates, functioning in a tissue-specific way (Nguyen and Frasch, 2006; Sokol and Ambros, 2005; Zhao et al., 2005, 2007). In this study, we use the purple sea urchin embryo, a deuterostomic invertebrate, to perform both loss-of-function and gain-of-function studies of miR-1 to further understand its role in developmental gene regulatory networks (GRNs).

The developmental processes of the sea urchin and humans are remarkably similar at the cellular and molecular level (Adonin et al., 2020). Similar to vertebrates, they utilize highly conserved signaling pathways such as the canonical Wnt (cWnt)/β-catenin signaling for anterior-posterior (AP) axis formation (Kiecker and Niehrs, 2001; Kimura-Yoshida et al., 2005; Logan et al., 1999; Wikramanayake et al., 1998) and BMP signaling for specification of the dorsal-ventral (DV) secondary body axis (Dal-Pra et al., 2006; De Robertis, 2006; Duboc et al., 2004; Floc'hlay et al., 2021; Khokha et al., 2005; Lapraz et al., 2009; Xu et al., 2014). Immediately after fertilization, maternal inputs, zygotic transcription, and signaling mechanisms help define distinct GRNs (Logan et al., 1999; Revilla-i-Domingo et al., 2007; Sherwood and McClay, 2001; Sweet et al., 2002; Wikramanayake et al., 1998). By the mesenchyme blastula stage, germ layer specification has already occurred; during gastrulation, the three germ layers are differentiated by cross-regulation among signaling pathways and GRN interactions (Davidson et al., 2002a; Davidson et al., 2002b; Oliveri et al., 2002;

Abbreviations: ALR, anterolateral rod; BR, body rod; BE-DVM, border ectoderm-dorsal ventral margin; cWnt, canonical Wnt; DE, dorsal ectoderm; Dpf, days post fertilization; DVC, dorsoventral connecting rod; EMT, epithelial to mesenchymal transition; GRN, gene regulatory network; Hpf, hours post fertilization; PMCs, primary mesenchyme cells; POR, postoral rod; TF, transcription factor; VE, ventral ectoderm; Vegf, vascular endothelial growth factor.

* Corresponding author. 323 Wolf Hall Newark, DE, 19716, USA.
E-mail address: jsong@udel.edu (J.L. Song).

https://doi.org/10.1016/j.ydbio.2024.01.010
Received 8 May 2023; Received in revised form 9 January 2024; Accepted 22 January 2024
Available online 28 January 2024

Revilla-i-Domingo et al., 2007; Yuh et al., 2002). We have also shown that post-transcriptional regulation mediated by miRNAs can also regulate skeletogenic primary mesenchyme cells (PMCs), immune cells, endodermally derived gut morphology, and neuronal development (Konrad and Song, 2022; Konrad et al., 2023; Sampilo et al., 2018, 2021; Song et al., 2011; Stepicheva and Song, 2015).

Although the body plans and structures of deuterostomes are diverse, the sea urchin embryo and vertebrates utilize conserved factors for analogous structures. For example, sea urchin skeletogenesis is thought to be analogous to vertebrate angiogenesis and vascularization since these processes utilize a common set of transcription factors (TFs) (Ets1/2, Erg, Hex, Tel, and FoxO) and signaling pathways (Vegf, Nodal/Bmp, Notch, and Angiopoetin) (Gildor et al., 2021; Morgulis et al., 2019). In response to the Vegf ligand in the ectoderm, the sea urchin *VegfR*-expressing PMCs initiate differentiation, patterning, and the formation of the skeletal rudiment (Adomako-Ankomah and Ettensohn, 2013; Duloquin et al., 2007; Morgulis et al., 2021). The migrating PMCs form a syncytium, connected by filopodial membranes between cell bodies where biomineralization enzymes form calcite granules (Bradham et al., 2004; Khor and Ettensohn, 2022; Winter et al., 2021). Similarly, the sea urchin larva utilizes similar TFs as vertebrates (FoxA, GataE, Xlox, Cdx) for gut differentiation (Annunziata et al., 2019; Annunziata and Arnone, 2014; Cole et al., 2009). The tripartite gut is compartmentalized with the cardiac, pyloric, and anal sphincters. For the nervous system, the sea urchin embryo uses orthologous neuronal transcriptional factors as those expressed in the vertebrate forebrain (Six3, ZIC2, Achaete-scute, NKX2.1 and FEZ) (Range and Wei, 2016; Wei et al., 2009). Thus, using the sea urchin as a simple and experimentally tractable organism, we can better understand complex molecular mechanisms that occur in vertebrate systems.

In the sea urchin, we take advantage of their well-characterized GRN to examine the function of miR-1 in early development. Previously, we found that miR-1 is one of the most highly expressed miRNAs in the purple sea urchin embryo (Song et al., 2011). The sea urchin has ~50 annotated miRNAs, which is a relatively small number in contrast to the 519 miRNAs in humans (Fromm et al., 2015; Kadri et al., 2011; Song et al., 2011; Wheeler et al., 2009). The sea urchin embryo contains a single miR-1, making it feasible to use this embryo to provide a deeper understanding of miR-1's function in development. Here we address the regulatory role of miR-1 in mesodermally-derived tissues of the sea urchin embryo, using loss- and gain-of-function perturbations. We discovered that miR-1 regulates circumpharyngeal muscle structures, skeletogenesis, and the positioning of PMCs. Using site-directed mutagenesis and reporter constructs, we identified that miR-1 modulates skeletogenesis by directly suppressing components of the PMC developmental GRN (*Ets1/2, Tbr,* and *VegfR7*), and *Nodal, Notch,* and *Wnt1* signaling components. Additionally, the gain-of-function of miR-1 resulted in more severe skeletal branching defects and PMC patterning than its loss-of-function.

2. Materials and methods

2.1. Animals

Adult purple sea urchin, *Strongylocentrotus purpuratus* (*Sp*), were obtained from Point Loma Marine Invertebrate Lab (Lakeside, CA) and Marinus Scientific, LLC (Long Beach, CA). Adult males and females were intracoelomically injected with 0.5 M KCl to obtain sperm and eggs. Filtered natural seawater (FSW) (collected from Indian River Inlet; University of Delaware) or artificial seawater (ASW) made from Instant Ocean© was used for embryo cultures incubated at 12 °C.

2.2. Cloning

To test potential miR-1 targets, we cloned transcripts containing miR-1 seed site (ACATTCC) downstream of luciferase constructs. To obtain 3′UTR of target genes, PCR primers or Fragment GENE DNA fragments (Genewiz, South Plainfield, NJ) were designed based on sequence information available from the sea urchin genome (echinobase.org) (Arshinoff et al., 2022) (Table S1). Amplified PCR products of *Bmp2/4, Ets1/2, Notch, Nodal,* and *Tbr* 3′UTRs were first cloned into ZeroBlunt vector (Thermo Fisher Scientific, Waltham, MA), and then subcloned into the *Renilla* luciferase (*R*luc) reporter construct. Wild type (WT) constructs of *IgTM* and *Nodal* were commercially synthesized. *VegfR7* and *Wnt1* 3′UTRs were previously cloned (Sampilo et al., 2021; Stepicheva and Song, 2015) (Table S1). Mutations were generated within the miR-1 seed sequences using the QuikChange Lightning or QuikChange Multi Site-Directed Mutagenesis Kit (Agilent Technologies, Santa Clara, California) to disrupt miR-1's binding and regulatory function (Staton and Giraldez, 2011; Stepicheva and Song, 2015). The predicted miR-1 seed sites (canonical site: 5′ ACATTCC 3′) within the 3′UTRs of *Ets1/2, Dri, Tbr, VegfR7, Notch, Nodal, Bmp2/4, Wnt1,* and *IgTM* were modified at the third and fifth base pair (Remsburg et al., 2019; Staton and Giraldez, 2011) (Table S1). We have previously demonstrated that truncated miRNA seed sequence differing in one nucleotide at the 5′ end is sufficient in miRNA-mRNA target recognition and function (Sampilo et al., 2021). *Nodal* and *Wnt1* contain truncated miR-1 sites (6 out of 7 bps), and *Bmp2/4* and *IgTM* contain mismatched miR-1 seed sites which differ in one nucleotide within the seed sequence (Table S1). Only two of the three potential miR-1 binding sites within *Nodal* 3′UTR were mutated due to sequence complexity. Firefly luciferase was used as a normalization control in the dual luciferase assay as previously described (Stepicheva and Song, 2015). Each of the construct sequences were verified by DNA sequencing (Genewiz, South Plainfield, NJ). Luciferase constructs containing *Ets1/2, VegfR7, Nodal,* and *IgTM* 3′UTRs were linearized with *Eco*RI, while *Tbr, Bmp2/4, and Wnt1* 3′UTRs were linearized with *Not*I. The luciferase constructs and *Firefly* luciferase mRNA were *in vitro* transcribed using the Sp6 mMessage machine kit (Ambion Inc, Austin, Texas). *In vitro* transcribed mRNAs were purified using Macherey-Nagel Nucleospin® RNA Clean-up kit (Macherey-Nagel, Bethlehem, PA) prior to injections.

2.3. Microinjections

Microinjections were performed as previously described (Cheers and Ettensohn, 2004; Stepicheva and Song, 2014) with modifications. All injection solutions were prepared in a 2.5 μl solution consisting of 20 % glycerol and 0.4 μg/μl of 10,000 MW neutral non-fixable Texas Red dextran (Thermo Fisher Scientific, Waltham, MA). Approximately 1–2 pL was injected into each newly fertilized egg based on the size of the injection bolus at about one-fifth of the egg diameter. miR-1 miRCURY LNA miRNA Power Inhibitor and miRCURY LNA miRNA mimic were obtained from Qiagen (Germantown, MD). miR-1 inhibitor (Hsa--miR-1-3p, ID# YI04100840; 5′- ACATACTTCTTTACATTCCA -3′) and miR-1 miRCURY LNA miRNA mimic (ID#YM00472818; 5′ UGGAAUGUAAAGAAGUAUGUAU 3′) were used at 10 μM, 30 μM and 40 μM concentrations. miRCURY LNA inhibitors are single-stranded antisense oligonucleotides with high specificity to their target miRNA (Davis et al., 2006; Orom et al., 2006; Roberts et al., 2006). Control embryos were injected with dextran with or without Cel-miR-39-3p LNA mimic (ID#YM00479902; 5′ UCACCGGGUGUAAAUCAGCUUG 3′) (not present in the sea urchin). miR-1 inhibitor and miR-1 mimic were co-injected at a 1:1 M ratio (40 μM miR-1 inhibitor + 40 μM miR-1 mimic) to test the specificity of miR-1 inhibitor.

2.4. Dual-luciferase quantification

The injection solutions for the dual-luciferase assay contained 20 % sterile glycerol, 0.4 μg/μl 10,000 MW Texas Red lysine-charged dextran, 100–200 ng/μl *Firefly* mRNA, and 100 ng/μl *R*luc mRNA (*Ets1/2, Dri, Tbr, VegfR7, Notch, Nodal, Bmp2/4, Wnt1,* and *IgTM*). 20–50 embryos were collected at the mesenchyme blastula stage (24 hpf). Dual

luciferase assays were performed using the Promega Dual-Luciferase Reporter (DLR™) Assay Systems with the Promega GloMax 20/20 Luminometry System (Promega, Madision, WI) (Sampilo et al., 2018, 2021; Stepicheva and Song, 2015). The *R*luc values were normalized to the Firefly signal to account for microinjection volume differences. *R*luc data with mutated miR-1 seed sites were normalized to the *R*luc with WT 3′UTR constructs. P-value was analyzed using Student's t-test. All error bars represent Standard Error of the Mean (SEM).

2.5. Immunofluorescence

Gastrulae and larvae were fixed in 4 % paraformaldehyde (PFA) (20 % stock; EMS, Hatfield, PA) in FSW overnight at 4 °C. Three PBS-Tween (0.05 % Tween-20 in 1X PBS) were performed, followed by 1 h block with 4 % sheep serum (MilliporeSigma, St. Louis, MO). 1D5 antibody was used at 1:50 to visualize PMCs (McClay et al., 1983) and diluted in PBS-Tween with 4 % sheep serum. Embryos were incubated overnight to 3 days at 4 °C and washed 3 times with PBS-Tween, followed by goat anti-mouse secondary antibody (Thermo Fisher Scientific, Waltham, MA) at 1:300 for 1 h at RT. Embryos were then washed 3 times with PBS-Tween and mounted on slides for confocal imaging. For visualization of DNA, embryos were counterstained with Hoechst dye (Lonza, Walkersville, MD), DAPI (Thermo Fisher Scientific, Waltham, MA), or VECTASHIELD® Antifade Mounting Medium with DAPI (Vector Laboratories, Burlingame, CA).

2.6. Whole mount and fluorescent in situ hybridization (WMISH and FISH)

The steps performed for fluorescence RNA *in situ* hybridization (F*I*SH) are described previously with modifications. The *Hsa*-miR-1-3p (ID# YD00619868; 5′ UGGAAUGUAAAGAAGUAUGUAU 3') miRCURY LNA detection probe (Qiagen, Germantown, MD) was used to visualize sea urchin miR-1 (at 0.5 ng/μl). The scramble-miR LNA negative control (ID# YD00699004; 5′ GTGTAACACGTCTATACGCCCA 3') detection probe was used as a negative control. Probes were incubated with embryos in hybridization buffer at 50 °C for 5–7 days as previously described with modifications (Konrad and Song, 2022; Sethi et al., 2014; Stepicheva and Song, 2015).

Partial coding sequences of *Bmp2/4, Nodal, Not1, Vegf3,* and *Wnt1* were cloned into ZeroBlunt vector to generate RNA probes (Thermo Fisher Scientific, Waltham, MA). Constructs were linearized using FastDigest™ (Thermo Fisher Scientific, Waltham, MA) and *in vitro* transcribed with DIG RNA labeling kit (Millipore Sigma, St. Louis, MO) (Table S2). *Vegf3* and *Wnt1* RNA probes were previously cloned (Sampilo et al., 2021; Stepicheva and Song, 2015). WM*I*SH was conducted according to previous publications (Arenas-Mena et al., 2000; Sampilo et al., 2021). Probes were used at 1 ng/μl and incubated at 50 °C for 5–7 days.

2.7. Imaging and phenotyping

Representative images were taken with Zeiss LSM 880 scanning confocal microscope using Zen software or ZEISS Observer Z1 using AxioVision software (Carl Zeiss Microscopy, LLC, White Plains, NY). For videos of gut contractions, live embryos were collected 5 dpf and mounted in FSW onto protamine sulfate (PS)-coated coverslips, creating a positively-charged surface (Stepicheva and Song, 2014). For live behavior examination, control, miR-1 inhibitor, and miR-1 mimic-injected embryos were mounted on the same multichambered PS-coated coverslip to avoid variability of environmental conditions and response. To examine the percentage of ingressed PMCs (Fig. S1), we used ZEISS Observer Z1 microscope with the AxioCam305 camera to take Z-stacks of brightfield images of *VegfR10* mRNA labeled cells along with DAPI staining to visualize the shape and position of PMCs to characterize their EMT state. To measure dorsoventral connecting rod (DVC) length or PMC migration, ZEISS Observer Z1 microscope was used to take Z-stacks of differential interference contrast (DIC). AxioVision or Zen 3.1 software (Carl Zeiss Microscopy, White Plains, NY) was used to measure the length of DVCs, PMC migration distance, and *in situ* expression domains of *Vegf3, Wnt1, Nodal, Not1,* and *Bmp2/4*. N is the total number of embryos examined unless otherwise stated. NS = not significant, $^{*}p < 0.05$, $^{**}p < 0.001$, $^{***}p < 0.0001$. All error bars represent SEM.

2.8. Real-time, quantitative PCR (qPCR)

To examine the levels of endogenous miR-1 expression within a developing embryo, 200–500 embryos were collected at various developmental stages. Purification of total RNA was done using miRNAeasy Micro Kit (QIAGEN, Germantown, MD). cDNA synthesis of 100 ng total RNA was performed with miRCURY LNA RT Kit (10 μl volume reaction) which adds a 5' universal tag of a poly(A) tail to mature miRNA templates (QIAGEN, Germantown, MD). cDNA template was diluted 1:10, and miRNA qPCR was performed using miRCURY LNA miRNA PCR Assays (QIAGEN, Germantown, MD) in QuantStudio 6 Real-Time PCR cycler system (Thermo Fisher Scientific, Waltham, MA). Sea urchin miR-200 were used as normalization controls due to its similar expression from the cleavage to the larval stages (Song et al., 2011). Results are shown as fold changes compared to the egg stage using the $Ct^{-2\Delta\Delta}$ method as previously described (Konrad and Song, 2022). miRCURY LNA miRNA PCR Primer Mix is against human miR-1 (Hsa-miR-1-3p).

To measure the transcriptional changes of genes that encode TFs of the skeletogenic GRN and biomineralization enzymes, we injected zygotes with control, miR-1 inhibitor, and miR-1 mimic. 100 of these blastulae were collected at 24 hpf. Total RNA was extracted by using the Macherey-Nagel Nucleospin® RNA Clean-up XS kit (Macherey-Nagel, Bethlehem, PA). cDNA was synthesized using iScript cDNA synthesis kit (Bio-Rad, Hercules, CA). qPCR was performed using 2.5 embryo equivalents for each reaction with the Fast SYBR or PowerUp Green PCR Master Mix (Thermo Fisher Scientific, Waltham, MA) in the QuantStudio 6 Real-Time PCR cycler system (Thermo Fisher Scientific, Waltham, MA). Results were normalized to the mRNA expression of ubiquitin and depicted as fold changes compared to control embryos using the $Ct^{-2\Delta\Delta}$ method as previously described to analyze the relative changes in gene expression (Stepicheva et al., 2015). Primer sequences were designed using the Primer 3 Program (Rozen and Skaletsky, 2000) and are listed in Table S3. 3–6 biological replicates were conducted. Statistical significance was calculated using two-tailed unpaired Student's t-tests.

3. Results

3.1. Expression of miR-1 peaks at the gastrula and larval stages with some enriched expression

To investigate the spatial and temporal expression of miR-1 throughout sea urchin development, we used miRNA real-time quantitative polymerase chain reaction (qPCR) and fluorescent *in situ* hybridization (F*I*SH). Using qPCR, we observed miR-1 transcript levels decreased 2-fold by 12 h post fertilization (hpf; early blastula) compared to the egg (Fig. 1A). By 48 hpf (gastrula) and 72 hpf (larvae), miR-1 transcript levels have increased over 10-fold. Using miR-1 F*I*SH, we observed miR-1 to be maternally expressed (Fig. 1B). At the 32-cell stage, the expression of miR-1 is enriched in the perinuclear region. Consistent with miRNA qPCR data, miR-1 expression peaks at the gastrula stage with ubiquitous expression and some enrichment in the mesenchymal cells, gut, and vegetal plate area. At the larval stage, miR-1 expression is still ubiquitous with slight enrichment in the gut and ciliary band (Fig. 1B).

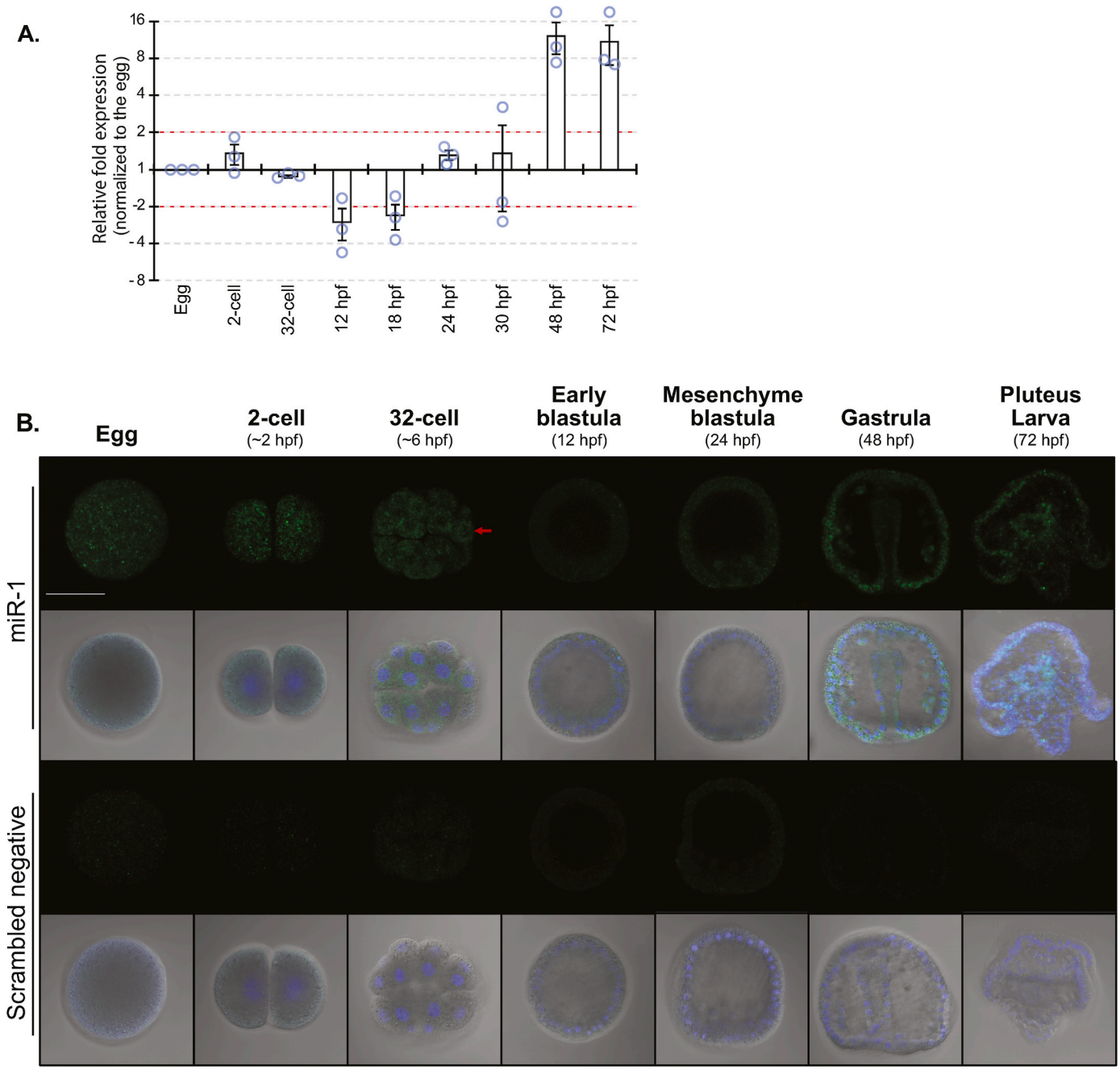

Fig. 1. miR-1 is dynamically expressed throughout development. (A) miR-1 expression is measured by relative miRNA RT-qPCR at various developmental stages. Red dashed lines indicate 2-fold expression difference. Blue circles represent datum points. 3 biological replicates. (B) F*ISH* was used to detect miR-1 at various developmental stages and counterstained with DAPI against DNA (blue). miR-1 is expressed perinuclearly in the 32-cell stage embryo (arrow). miR-1 has increased expression during gastrula stage with enrichment in the mesenchymal cells, gut, and vegetal plate area. miR-1 is enriched in the larval ciliary band and gut. 3 biological replicates. Scale bar = 50 μm.

3.2. Perturbation of miR-1 results in circumpharyngeal muscle defects

To examine the function of miR-1 in early development, we injected miR-1 inhibitor for loss-of-function studies or miR-1 mimic for gain-of-function studies. miR-1 miRCURY LNA inhibitor is complementary in sequence with miR-1, so it binds to the endogenous miR-1 to inhibit its function in the embryo. miRCURY LNA mimics are double stranded RNA that are designed to be recognized by the RNA-induced silencing complex (RISC) and consist of three RNA strands, including the specific miRNA and two segmented passenger strands that are rapidly degraded, once the specific miRNA is incorporated into the RISC complex (Owczarzy et al., 2011). Thus, the miR-1 mimic should not bind to the miR-1 LNA inhibitor in co-injection rescue experiments. Since miR-1 is enriched and plays a function in the vertebrate muscle, we examined the effect of miR-1 perturbations on the structure of the circumpharyngeal muscles that surround the larval gut (Fig. 2). As indicated by the miR-1 F*ISH* followed by miR-1 inhibitor injection, miR-1 level in the miR-1 inhibited embryos was greatly reduced compared to the control; however, this is a qualitative assessment as conventional F*ISH* is not quantitative (Fig. 2A). The number of filamentous actin-rich fibers (F-actin) within the muscle fiber ring was significantly decreased and less structured in both miR-1 inhibitor and miR-1 mimic-injected larvae compared to the control. Almost 20 % of miR-1 mimic-injected larvae had a complete loss of detectable F-actin (Fig. 2B). The miR-1

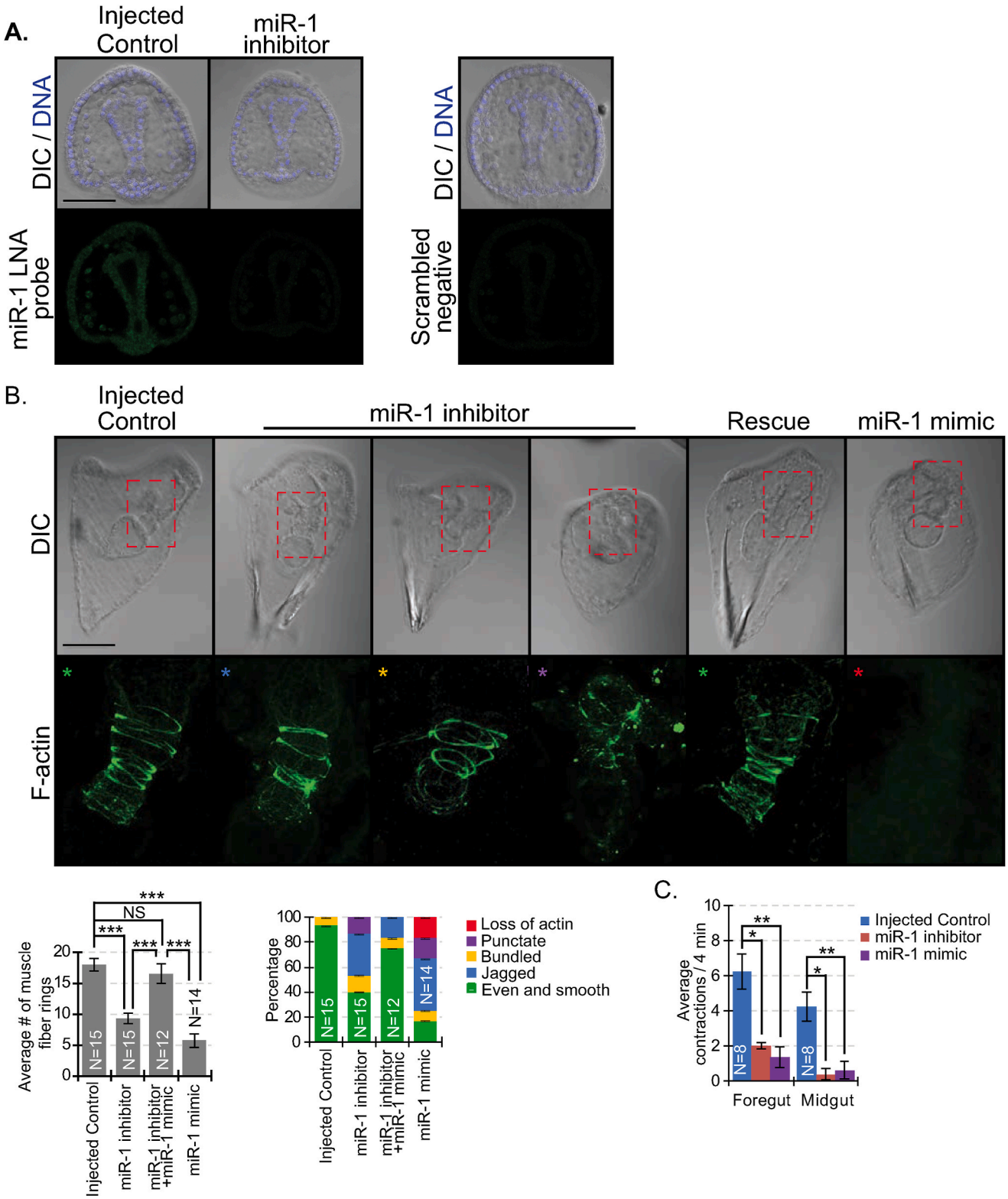

Fig. 2. Perturbation of miR-1 results in circumpharyngeal muscle morphological defects. (A) Zygotes injected with miR-1 inhibitor or control (40 μM) were subjected to miR-1 or scrambled FISH RNA probes. Endogenous miR-1 is greatly reduced in miR-1 inhibitor-injected embryos. N = 20. 3 biological replicates (B) Circumpharyngeal muscles were labeled with phalloidin to detect F-actin. Z-stack of confocal images were taken to count muscle fiber rings. Compared to control, miR-1 perturbed larvae exhibited less or a complete loss of F-actin, in addition to irregular F-actin morphology (boxed areas). miR-1 inhibitor induced defects were rescued by co-injection of miR-1 mimic (40 μM). Colored asterisks correspond to phenotypes in the bar graph. NS = not significant, *$p < 0.05$, **$p < 0.001$, ***$p < 0.0001$. All error bars represent SEM. 4 biological replicates. Student's t-test. Scale bar = 50 μm. (C) miR-1 perturbed larvae exhibit significantly less contractions of the foregut and the midgut compared to control. *$p < 0.05$, **$p < 0.001$. All error bars represent SEM.

inhibitor-induced defects were rescued by co-injection with the miR-1 mimic, indicating that the muscle fiber defects are due to miR-1 perturbation. Interestingly, both miR-1 inhibitor and miR-1 mimic-injected larvae have significantly fewer foregut and hindgut contractions compared to the control, indicating a potential defect in gut functions (Movies 1–3) that may be related to their circumpharyngeal muscle structures.

Supplementary video related to this article can be found at https://doi.org/10.1016/j.ydbio.2024.01.010

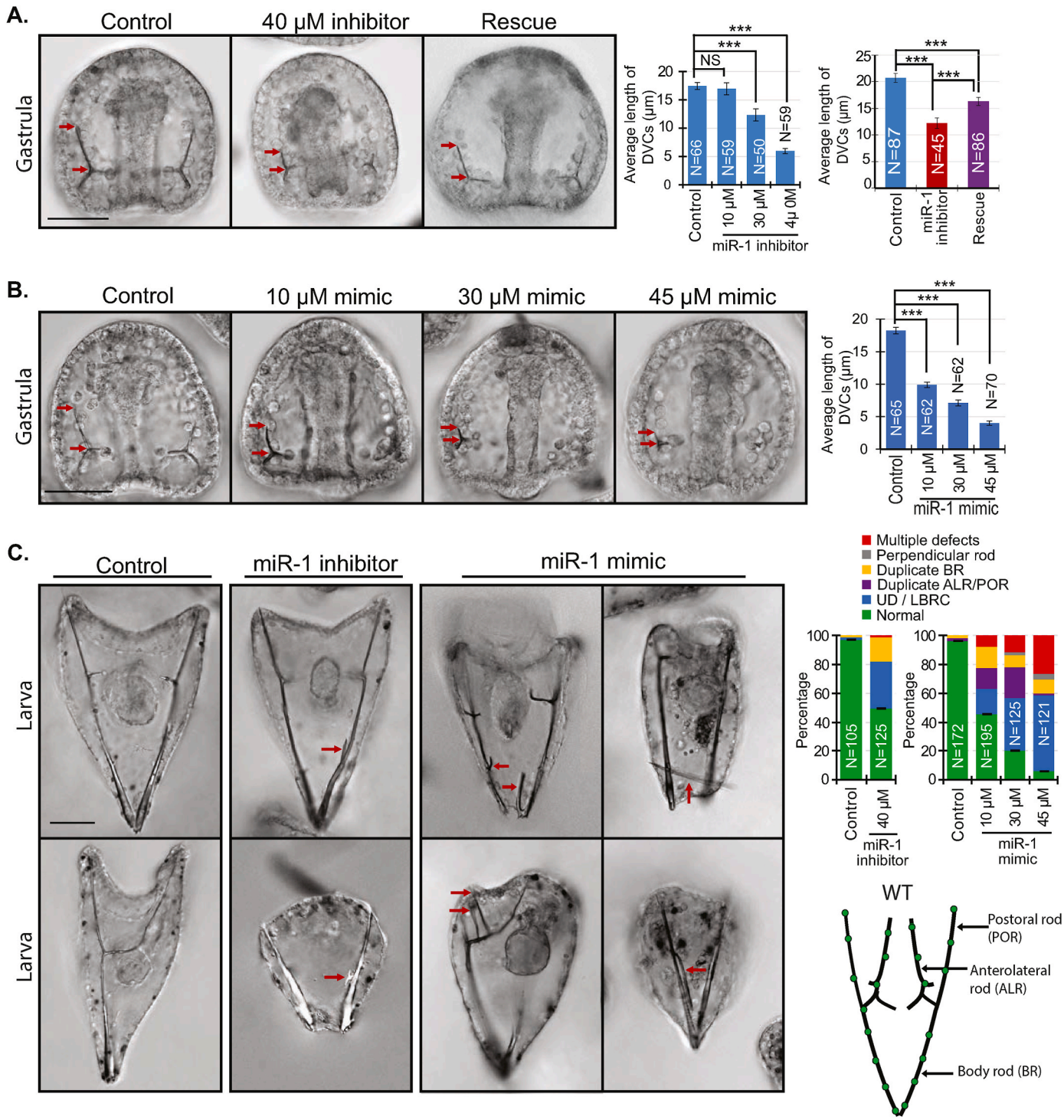

Fig. 3. Perturbation of miR-1 results in the shortening of the DVCs and abnormal skeletal branching. (A) miR-1 inhibitor was injected at various concentrations, resulting in decreased DVC length in a dose-dependent manner. Shortened DVCs can be partially rescued by co-injection of miR-1 inhibitor with the miR-1 mimic. Arrows indicate the length of DVCs. NS = not significant, ***$p < 0.0001$. All error bars represent SEM. (B) miR-1 mimic-injected embryos had a dose-dependent decrease of DVCs. N is the total number of embryos examined. NS = not significant, ***$p < 0.0001$. All error bars represent SEM. Student's t-test. Scale bar = 50 μm. (C) miR-1 inhibitor-injected larvae exhibited duplicated Body Rod (BR) branching, lack of BR convergence (LBRC), and underdeveloped (UD) larvae. miR-1 mimic-injected embryos were underdeveloped and exhibited severe defects of duplicated branching (arrows) off the Postoral Rods (PORs), Anterolateral Rods (ALRs), and/or BRs in a dose-dependent manner. 3 biological replicates. Scale = 50 μm.

3.3. Perturbation of miR-1 results in skeletal defects

Although the sea urchin larval skeleton is not myogenic, skeleton is mesodermally-derived similar to muscles. Since miR-1 regulates mesodermally-derived muscles (Mansfield et al., 2004; McCarthy, 2011; Sokol and Ambros, 2005; Wienholds et al., 2005; Zhao et al., 2005), we also examined other mesodermally-derived cell types, including the PMCs. We found both miR-1 loss-of-function and gain-of-function resulted in a significant delay of PMC ingression during gastrulation (Fig. S1); however, this delay is transient as larval skeleton is formed (Fig. 3). miR-1 perturbed embryos had an average of three PMCs less than control embryo, not likely to make a significant difference in skeletogenesis (Fig. S1).

During gastrula stage, we observed that miR-1 inhibitor and miR-1 mimic injections resulted in decreased length of DVCs as well as all radii of the tri-radiate in a dose-dependent manner (Fig. 3A and B). miR-1 inhibitor-induced skeletal defects were partially rescued by co-injection of a miR-1 mimic, indicating that this defect is specifically induced by miR-1 inhibition (Fig. 3A). In addition, miR-1 inhibitor-injected larvae were underdeveloped, lacked body rod (BR) convergence, and/or occasionally exhibited duplicate BR branching (Fig. 3C). On the other hand, although miR-1 mimic-injected gastrulae have significantly shortened radii of the tri-ratiate, miR-1 mimic-injected larvae had a dose-dependent severity of abnormal and supernumerary skeletal branching off the postoral rods (POR), anterolateral rods (ALR), and BRs (Fig. 3C). We also observed independent skeletal elements developed perpendicular to the larval BRs. Overall, these results indicate that miR-1 plays a critical role in the initial formation and elongation of the skeletal spicules and that miR-1 mimic injections induced a more severe larval skeletal defect than miR-1 inhibitor injections.

3.4. Perturbation of miR-1 results in PMC patterning defects

Since we observed skeletal branching defects (Fig. 3), we examined the effect of miR-1 perturbations on the patterning of PMCs, which are cells that make the skeleton (Ettensohn and McClay, 1986). In miR-1 inhibitor-injected gastrulae, we found that while the patterning of PMCs was not greatly affected, PMCs were clustered posteriorly and had less anterior migration compared to the injected control using PMC specific antibody and *VegfR10* RNA probe (Fig. 4Ai-ii). This decreased migration in miR-1 inhibitor-injected embryos was partially rescued by co-injection of miR-1 mimic, indicating that this defect is due to inhibition of miR-1. miR-1 inhibitor-injected larvae had occasional PMCs positioned off a skeletal branch (red arrow in Fig. 4Ai) and an occasional duplicated body rod (Fig. 4C), indicating that miR-1 inhibition is likely to mildly affect biomineralization rather than PMC patterning. In miR-1 mimic-injected gastrulae, several PMCs migrated to the animal pole (referred to as scattered PMCs) (arrows in Fig. 4Bi-ii). Interestingly, miR-1 mimic-injected larvae also had several PMCs migrate off skeletal branches with apparent syncytium to the main skeletal body (white arrow in Fig. 4Cii). The defective migration and patterning of PMCs in miR-1 mimic-injected embryos with various duplicated branching suggest that overexpression of miR-1 disrupts skeletal patterning cues and promote ectopic branching formation (Fig. 4Cii).

3.5. miR-1 directly targets components of skeletogenic GRN and signaling pathways

To reveal the regulatory molecular mechanism of miR-1, we bioinformatically searched for potential miR-1 seed sites within transcripts that encode regulators of the PMC GRN and key components of signaling pathways (Fig. 5A). We examined the direct suppression of miR-1 of *Ets1/2*, *Dri*, *Tbr*, *VegfR7* of the PMC GRN (Kurokawa et al., 1999; Oliveri et al., 2002; Rottinger et al., 2004; Stepicheva and Song, 2015), *Nodal*, *Bmp/4*, and *Wnt1* of the signaling pathways that may impact PMCs (Duboc et al., 2004, 2010; Sampilo et al., 2021; Saudemont et al., 2010), and *IgTM* which has been found to play an important role in skeletal morphogenesis by regulating the number of initial branches that arise within each skeletal primordium (Ettensohn and Dey, 2017). We cloned the 3′UTRs of these genes downstream of *Renilla* luciferase (*R*luc) and compared luciferase levels of *Renilla* luciferase reporter mRNAs containing WT or mutated miR-1 binding sites with control Firefly luciferase flanked by *Xenopus β-globin* UTRs (Stepicheva and Song, 2015). The *R*luc readout was normalized to the Firefly luciferase to account for injection differences. miRNA's binding to the 3′UTR of a target gene would silence its translation, whereas mutating the miRNA binding sites would abolish miRNA binding to 3′UTR of a target transcript, leading to increased translation of luciferase. We determined that miR-1 directly suppresses luciferase reporters bearing the 3′UTRs of *Ets1/2, Tbr, VegfR7, Notch, Nodal,* and *Wnt1*. miR-1 may have weak miRNA-mRNA binding affinity with *Dri* (Fig. 5B).

3.6. miR-1 mimic-injections result in ectopic expression domains of several factors

To identify the molecular mechanism of how miR-1 regulates skeletogenesis, we examined the spatial expression of key factors involved in PMC patterning, including *Vegf3, Wnt1, Nodal, Not1,* and *Bmp2/4* in gastrulae (Fig. 6). In miR-1 inhibitor-injected gastrulae, the lateral and vegetal expression domains of *Vegf3* were significantly decreased compared to control (Fig. 6A). Concurrently, the vegetal expression domains of *Nodal* and *Not1* were expanded, without expression domain change of *Bmp2/4* (Fig. 6Bi, iii). In miR-1 mimic-injected gastrulae, the lateral expression of *Vegf3* had no expression domain change; however, its vegetal expression domain was significantly expanded (Fig. 6Aii, iii). In contrast to miR-1 inhibitor-injected embryos, *Nodal, Not1,* and *Bmp2/4* expression domains were decreased in the vegetal expression domains of the miR-1 mimic-injected embryos, while the expression domain of *Wnt1* was increased compared to control (Fig. 6Bii). In general, miR-1 loss- and gain-of-function resulted in reciprocal changes in *Vegf3*, *Nodal*, and *Not* expression domains.

3.7. miR-1 regulates the expression of key skeletogenic transcripts

To identify the underlying molecular mechanism that led to PMC patterning and skeletal branching defects, we examined the relative expression levels of transcripts that encode PMC specification and patterning (*Ets1/2, Dri, Tbr, Snail, Nodal, Bmp2/4, Not1, Vegf3, Wnt1, FgfA* and *CDC42*) (Adomako-Ankomah and Ettensohn, 2013; Duboc et al., 2010; Duloquin et al., 2007; Rottinger et al., 2004, 2008; Sepúlveda-Ramírez et al., 2018), biomineralization enzymes (*P19, p58A, SM30, SM50*) (Adomako-Ankomah and Ettensohn, 2011; Cheers and Ettensohn, 2005; Livingston et al., 2006), PMC-specific cell surface protein *Msp130* (Leaf et al., 1987), PMC adhesion protein *KirrelL* (Ettensohn and Dey, 2017), and markers of dorsal PMCs (*Tbx2/3* and *GataC*) (Duboc et al., 2010) (Fig. 7). In general, miR-1 inhibited blastulae have increased expression for genes that encode TFs involved in PMC GRN (*Ets1/2*, *Dri*, *Tbr*, *Snail*) and *Notch*, whereas miR-1 mimic-injected blastulae have decreased expression for these same transcripts. Specifically, miR-1 inhibited blastulae have significantly increased *Tbr* mRNA compared to the injected control; significantly decreased *GataC* and *Tbx2/3* mRNAs expressed in dorsal PMCs; significantly decreased *p19*, *SM50*, *IgTM*, *Kirrel*, and *FgfA* mRNAs. In contrast, miR-1 mimic-injected blastulae have significantly decreased *p58A* mRNA, significantly increased *Wnt1* mRNA, and significantly decreased *Bmp2/4*, *Not1*, *Notch*, and *Cdc42* mRNAs (Fig. 7). Both miR-1 inhibitor and miR-1 mimic-injected embryos have no change or decreased expression of genes involved in biomineralization, suggesting that miR-1 indirectly regulates biomineralization transcripts to impact skeletogenesis.

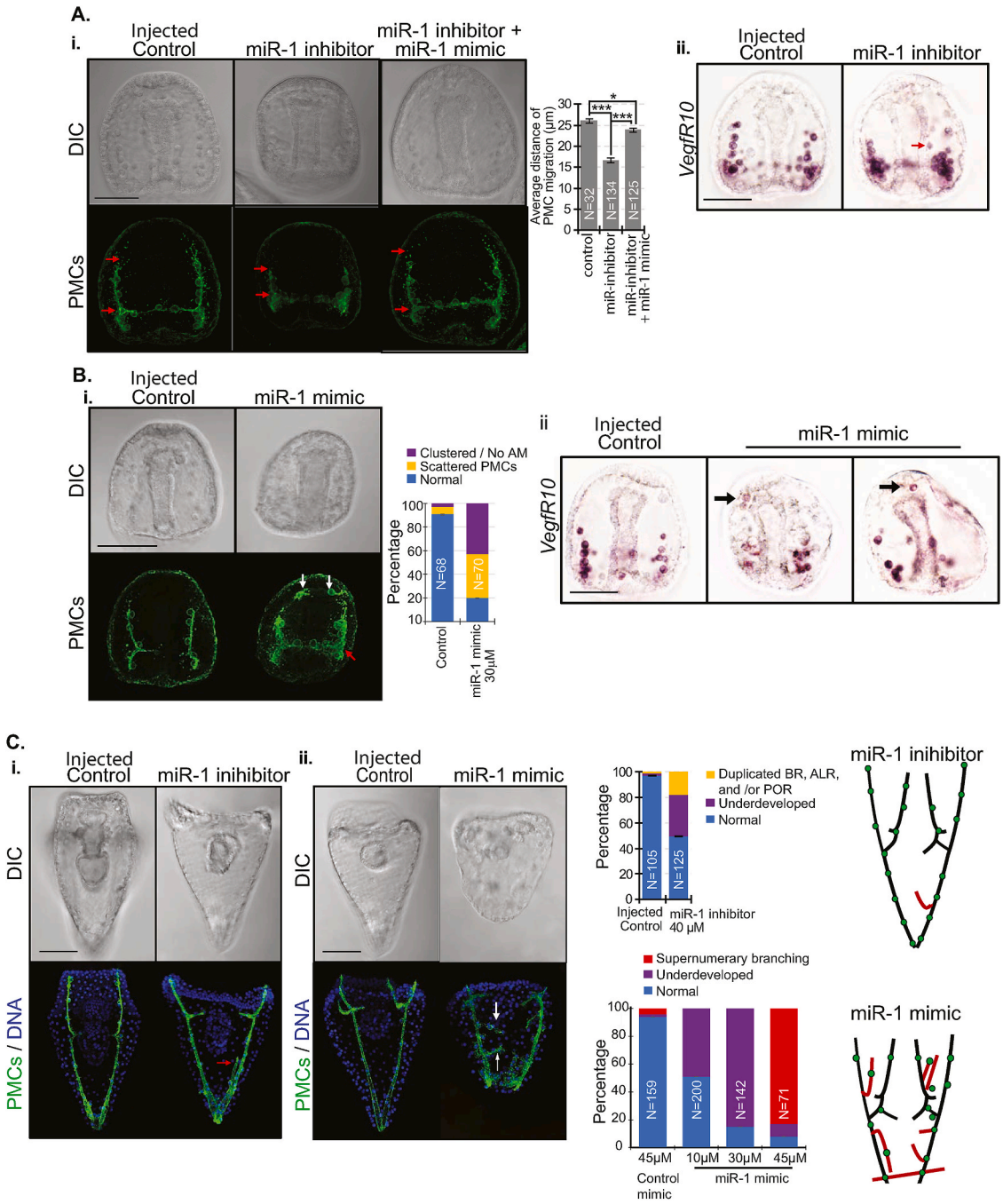

Fig. 4. Perturbation of miR-1 results in ectopic PMC patterning. Gastrulae were immunolabeled with 1D5 PMC antibody (McClay et al., 1983) or hybridized with the *VegfR10* RNA probe. (Ai) PMCs recognized by 1d5 antibody in miR-1 inhibitor-injected gastrulae exhibit less anterior migration (delineated by red arrows) compared to the control that was able to be partially rescued by co-injection of miR-1 mimic. Student's t-test. 3 biological replicates. (Aii) *VegfR10*-expressing cells also exhibit clustering and lack of anterior migration compared to control, similar to immunolabeling with the 1D5 antibody. Occasional PMCs positioned off a skeletal branch (red arrow). (Bi) Control and miR-1 mimic-injected gastrulae were immunolabeled with 1d5 antibody for PMCs. miR-1 mimic-injected gastrulae exhibited scattered PMCs (white arrows) that have migrated near animal pole and clustered PMCs at the posterior end of the embryo with no anterior migration (AM) (red arrow). (Bii) miR-1 mimic-injected embryos have *VegfR10*-expressing cells at the most anterior end of the embryo compared to control, similar to the 1d5 immunolabeling results. (Ci) Larvae were immunolabeled with 1D5 antibody for PMCs and counterstained with DAPI (blue). Compared to control, miR-1 inhibitor-injected larvae exhibited duplicated branching off the BR (arrow). (Cii) miR-1 mimic-injections resulted in severe PMC patterning defects, correlating to abnormal skeletal branching. Scale = 50 µm.

4. Discussion

miR-1 is a myomiR that has been found to regulate muscle development (Mansfield et al., 2004; McCarthy, 2011; Sokol and Ambros, 2005; Wienholds et al., 2005; Zhao et al., 2005). In this study, we found miR-1 to regulate circumpharyngeal muscles, the proper formation of the larval skeleton, and the patterning of mesodermally-derived PMCs. Our results indicate that miR-1 regulates skeletogenesis, likely via its suppression of components of the PMC GRN (*VegfR7*, *Ets1/2* and *Tbr*) and *Nodal* and *Wnt1* signaling components. In addition, miR-1 indirectly regulates biomineralization transcripts and *Vegf3* to potentially impact spicule formation and PMC patterning, respectively.

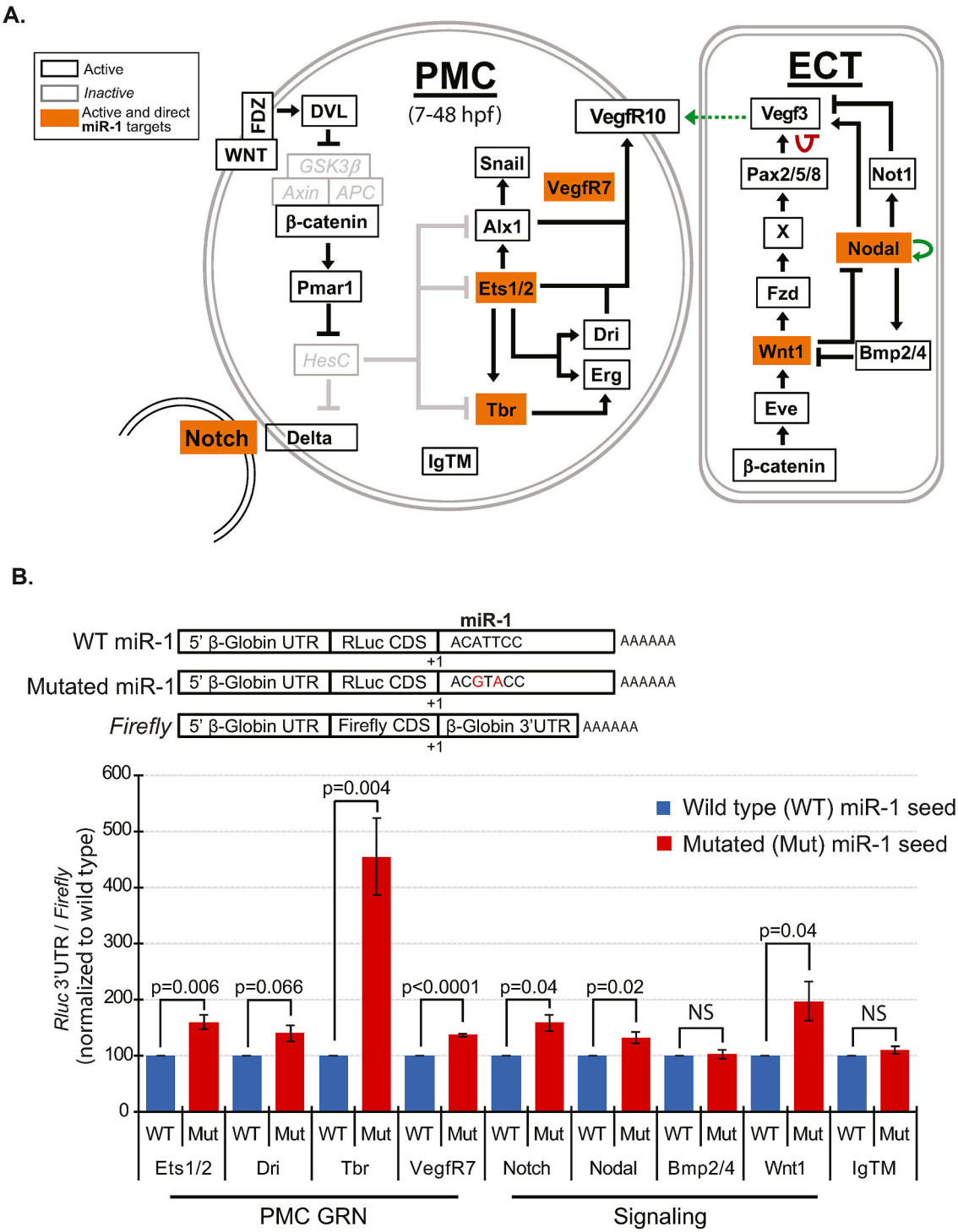

Fig. 5. miR-1 targets multiple components skeletogenic GRN and signaling pathways. (A) Schematic of simplified PMC GRN is shown. PMCs are specified by the Wnt/β-catenin signaling pathway which activates the transcriptional repressor *Pmar1,* leading to the activation of skeletogenic TFs *Ets1/2*, *Tbr*, *Alx1*, *Dri* and *Erg*, as well as other endodermally and mesodermally-derived TFs (not shown). In the ectoderm (ECT), Wnt/β-catenin signaling activates *Eve* which in turn activates *Wnt1*. Nodal in the ventral ectoderm activates BMP signaling to restrict *Wnt1* to the posterior-ventral side while Wnt1 prevents Nodal expression in the posterior region. Nodal activates *Not1,* and Not1 represses *Vegf3* in the ventral ectoderm, thus restricting *Vegf3* expression to the two lateral ectodermal domains. Validated miR-1 targets are highlighted in orange. (B) Schematics of the luciferase constructs are shown. 3′UTR (indicated by position +1) of select transcripts were cloned downstream of *Renilla* luciferase vector. The predicted reverse complement of the miR-1 seed sequence (ACATTCC) was altered at nucleotides 2 and 5 using site-directed mutagenesis. Dual luciferase assays with constructs with WT or mutated miR-1 sites were used to validate miR-1 targets. miR-1 directly suppresses *Ets1/2, Tbr, VegfR7, Notch, Nodal* and *Wnt1*. NS = not significant. All error bars represent SEM. Student's t-test.

miR-1 expression is enriched in multiple tissues of the gastrulae and larvae (Fig. 1). The expression pattern of miR-1 may reveal its regulatory mechanism. In vertebrates, miR-1 is enriched in muscle lineages and may function as a developmental switch when it is specifically expressed in cardiac and skeletal tissues. In invertebrates, miR-1's expression is broader with more variable functions, including regulation in immunity

by suppression of clathrin during phagocytosis in shrimp (Liu et al., 2014), neuromuscular junction in nematodes (Simon et al., 2008), midgut regeneration in fruit fly (Takemura et al., 2021), and sex-determination in oriental fruit fly (Peng et al., 2020). Our results indicate that the sea urchin miR-1 has a broader expression with more diverse functions than vertebrates, including in circumpharyngeal muscle structures and skeletal components.

We observed that miR-1 perturbed larvae have decreased number of F-actin muscle fiber rings (Fig. 2B). The defective gut contractions in miR-1 perturbed larvae may be due to problems with the muscle fibers and/or neural coordination (Fig. 2C). Previous work has shown Delta/Notch signaling to play critical roles in vertebrate myogenesis (Conboy and Rando, 2002; Kopan et al., 1994; Schuster-Gossler et al., 2007), and knockdown of *Delta* or introducing a dominant negative version of *Notch* that lacks the Notch intracellular domain in the sea urchin embryos resulted in decreased muscle fibers (Sherwood and McClay, 1999; Sweet et al., 2002). Using site-directed mutagenesis and dual luciferase assays, we determined that miR-1 directly suppresses reporter bearing the 3′UTR of *Notch*. Even though miR-1 inhibition did not significantly alter transcript level of *Notch*, miR-1 mimic injection resulted in a significant decrease of *Notch* mRNA, suggesting that miR-1's regulation of *Notch* may be in part via inducing transcript degradation (Fig. 7). Since Notch receptor functions with Delta ligand, changes in *Notch* mRNA alone is not likely to affect the signaling and thus not likely to explain the muscle phenotypes induced by miR-1 perturbations. In addition, although perturbations of the sonic hedgehog pathway in the sea urchin embryo led to disorganized circumesophageal muscle causing an inability to swallow (Walton et al., 2009), we did not identify potential miR-1 binding sites within *Sonic Hedgehog*, *Smoothened*, or *Patched* transcripts.

Another mesodermally-derived tissue that is regulated by miR-1 is the larval skeleton. Our results indicate that all radii of the tri-radiate at late gastrula stage are significantly shortened in embryos injected with either miR-1 inhibitor or miR-1 mimic (Fig. 3A and B). 40 % of these miR-1 mimic-injected gastrulae embryos have PMCs that migrated all the way to the anterior region of the gastrulae (Fig. 3B and 4B), indicating that these mispatterned PMCs do not seem to contribute to skeletal initiation. The shortened tri-radiates phenotype in the miR-1 perturbed gastrulae seems to be a transient effect, since both miR-1 inhibitor and mimic-injected larvae have elongated skeletal structures and ectopic branching (Fig. 3C).

Of note is that the penetrance of miR-1 mimic seems to be better than the miR-1 inhibitor (Fig. 3). This difference in penetrance of the inhibitor and miR-1 mimic is potentially due to the difference in how they are synthesized, designed and prepared by the manufacturer. miRCURY LNA inhibitor is a RNA complementary to miR-1; however, how many LNA residues are designed into the LNA inhibitor sequence is proprietary. On the other hand, miRCURY LNA mimics are double stranded RNA that are designed to be recognized by the RNA-induced silencing complex (RISC) and consist of the miRNA itself with two passenger strands that are rapidly degraded once the specific miRNA is incorporated into the RISC complex (Owczarzy et al., 2011; Qiagen, 2018). Due to these differences, the penetrance of the miR-1 mimic seems to be better than the miR-1 inhibitor.

In general, results suggest that miR-1 inhibition leads to mild biomineralization defects and miR-1 overexpression leads to perturbation of PMC patterning cues (Figs. 3 and 4). Results indicate that p19 and SM50 are significantly decreased in miR-1 inhibited blastulae and p58A is significantly decreased in miR-1 mimic-injected blastulae (Fig. 7). The decreased biomineralization transcripts in miR-1 inhibited and overexpressed blastulae may explain the shortened skeletal length in these gastrulae (Figs. 3 and 7). The result is seemingly contradictory in that miR-1 mimic-injected gastrulae have significantly shortened tri-radiates but have multiple duplicated branching in the larval stage (Fig. 3C). However, we do not know the level of these biomineralization transcripts in gastrula and larval stages. In addition, the change in miR-1's expression pattern throughout early development suggests that miR-1's regulation of biomineralization genes may change throughout development (Fig. 1B). There may also be unknown factors that miR-1 suppresses that is involved in providing negative signals to skeletal branching, as miR-1 mimic induces supernumerary branching (Fig. 3C).

To understand how miR-1 may be regulating PMC development, we used site-directed mutagenesis and dual luciferase assays to identify miR-1 target transcripts (Fig. 5). We found miR-1 to directly suppress reporters containing 3′UTRs of *Ets1/2, Tbr,* and *VegfR7* of the PMC GRN, and *Notch, Nodal,* and *Wnt1* of signaling pathways (Fig. 5). We analyzed the spatial expression of factors that may affect PMC patterning (Fig. 6), as well as the level of transcripts that encode proteins that affect skeletogenesis (Fig. 7). Since PMCs are mainly responsible for the formation of the larval skeleton (Ettensohn and McClay, 1986), we examined the patterning of PMCs (Fig. 4). It was striking that PMCs are mispatterned in miR-1 mimic-injected embryos (Fig. 4B). Some of these PMCs in miR-1 mimic-injected larvae appear to be mispatterned to areas where we observed spurious skeletal branches in the larvae (Fig. 4C), indicating a disruption of patterning cues.

For both miR-1 inhibitor and miR-1 mimic-injected blastulae, the percentage of PMCs undergoing EMT is significantly and consistently less than the control (Fig. S1). Since we observe that at a later time point PMCs ingress into the blastocoel, this EMT delay is transient. However, even though the delay of PMC ingression is transient (Fig. S1), this delay could potentially affect PMC patterning by disrupting the time and distance-sensitive interaction between *VegfR10*-expressing PMCs and the *Vegf3* ligand expressed in the ectoderm, as *Vegf3* expression becomes restricted to the Veg1 ectoderm by 30 hpf (early gastrula) (Li et al., 2014).

In miR-1 inhibited gastrula, *Vegf3*, *Nodal*, and *Not1* had significant expression domain changes that were reciprocal to that of miR-1 mimic-injected embryos. The loss-of-function of *Vegf* inhibits skeleton formation (Duloquin et al., 2007). Thus, the decreased expression domain of *Vegf* in miR-1 inhibited embryos is consistent with overall reduced biomineralization in these gastrulae (Fig. 6A and 7). On the other hand, miR-1 mimic-injected embryos have expanded *Vegf* that may contribute to the duplicated skeletal element branching observed later in those larvae. Interestingly, *Vegf3* transcript level at blastula stage was not altered in both miR-1 inhibited or overexpressed blastulae (Fig. 7), suggesting that miR-1 may regulate factors that restrict the expression domain of *Vegf3*. In zebrafish, miR-1 has been found to negatively regulate angiogenesis during development by repressing *VegfAa* (Stahlhut et al., 2012). We bioinformatically identified potential miR-1's binding site within the sea urchin *Vegf3* transcript. Thus, if miR-1 directly regulated *Vegf3*, it would be likely affecting its protein level, since its transcript was not significantly altered upon miR-1 perturbation (Fig. 7).

We also observed that the expression domain of *Nodal* is significantly increased in miR-1 inhibited gastrulae and significantly decreased in miR-1-mimic injected gastrulae, further suggesting that miR-1 regulates *Nodal* (Fig. 6B). Although the level of *Nodal* transcripts was not greatly altered in miR-1 mimic-injected blastulae assessed with qPCR, we observed a significant >3-fold decrease of Nodal's known target, *Not1* (Fig. 7) (Li et al., 2012; Materna et al., 2013). This result suggests that miR-1 mimic-injected embryos may have decreased Nodal protein, resulting in decreased *Not1* transcripts (Fig. 7). This also suggests that miR-1 regulates *Nodal* at the post-transcriptional level. Prior studies have shown that Nodal activates the expression of itself, *Not1*, *Bmp2/4*, and *Vegf3* in the ventral ectoderm of the early blastula (Li et al., 2012). Also, *Not1* knockdown led to expanded *Vegf3* expression in the ventral ectoderm (Li et al., 2012). Therefore, although our skeletal defects do not phenocopy Nodal's loss-of-function which resulted in broad perturbance of the skeleton, the level of miR-1 modulation of *Nodal* may indirectly impact the *Vegf3* expression domain in the ventral ectoderm (Duboc et al., 2004, 2010; Layous et al., 2021; Li et al., 2012; Saudemont et al., 2010).

We also observed an expanded expression domain of *Wnt1* in miR-1

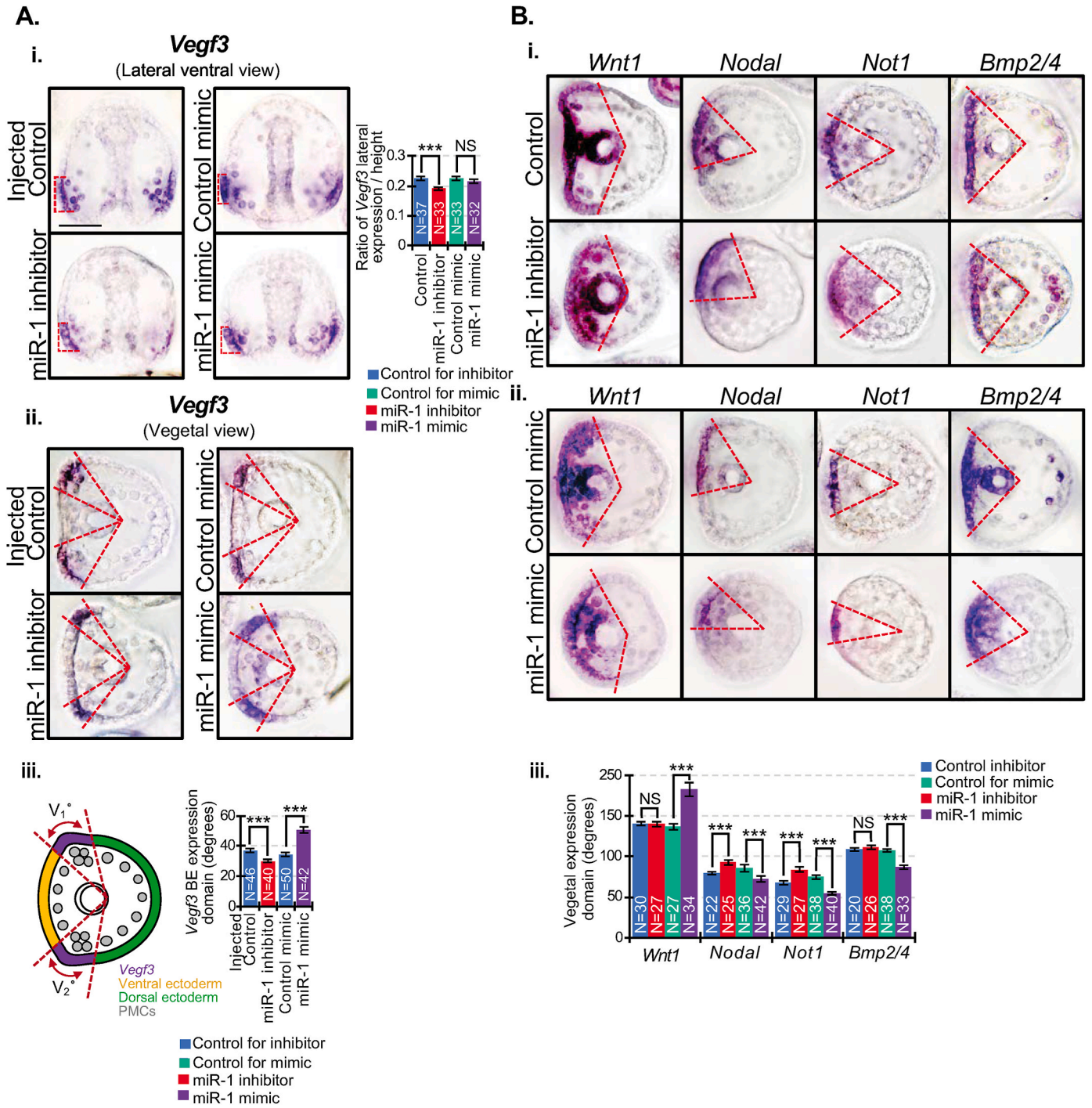

Fig. 6. Perturbation of miR-1 results in ectopic expression domains. The expression domains of *Vegf3, Wnt1, Nodal, Not1* and *Bmp2/4* were assessed. (Ai) The lateral expression domain of *Vegf3* (red dashed lines) was decreased in miR-1 inhibited gastrulae compared to the control, whereas the lateral expression domain of *Vegf3* in miR-1 mimic-injected embryos did not change compared to the injected control. (Aii) miR-1 inhibited gastrulae have decreased ventral *Vegf3* expression domain compared to the control. The vegetal expression domain of *Vegf3* of miR-1 mimic-injected embryos was significantly expanded compared to the injected control embryos. (Aiii) The graph indicates the ventral expression domain of *Vegf3* was measured in injected control, miR-1 inhibitor, and miR-1 mimic-injected gastrulae. (Bi) In miR-1 inhibitor-injected gastrulae, vegetal expression domains of *Nodal* and *Not1* were expanded, while the expression domains of *Bmp2/4* and *Wnt1* were not altered. (Bii) In miR-1 mimic-injected embryos, *Nodal, Not1* and *Bmp2/4* vegetal expression domains decreased, while the expression domains of *Wnt1* and *Vegf3* expanded. (Biii) The graph indicates the expression domains of *Wnt1*, *Nodal*, *Not1*, and *Bmp2/4* of injected control, miR-1 inhibitor and miR-1 mimic-injected embryos. N is the number of domains measured. Student's t-test. ***$p < 0.001$. NS = not significant. 2–3 biological replicates. Scale = 50 μm. SEM is graphed.

mimic-injected embryos. Wnt1 can activate its own transcription and is part of highly cross-regulated positive feedback circuitry (Cui et al., 2014; Sampilo et al., 2021). miR-1 mimic-injected embryos resulted in significant increased levels of *Wnt1* mRNA, suggesting that *Wnt1* transcript is altered in response to other factors regulated by miR-1. miR-1 mimic-injected embryos resulted in significantly decreased *Bmp2/4* (Fig. 7). Since miR-1 does not regulate *Bmp2/4*, this regulation is likely to be indirect (Fig. 5). The significant expression domain

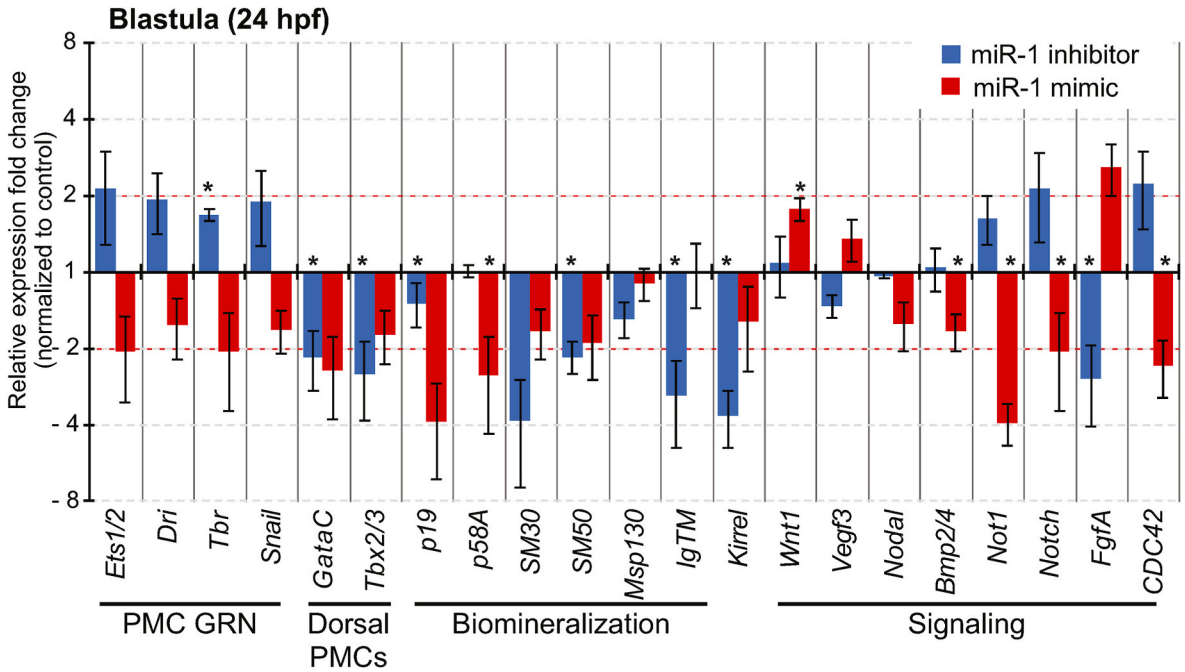

Fig. 7. miR-1 regulates key skeletogenic transcripts. The expression levels of key transcripts encoding factors important for PMC development were assessed by qPCR at the mesenchyme blastula stage. The dashed red line indicates 2-fold differences. 3–5 biological replicates were conducted. Each replicate contains 100 embryos. Student's t-test was used. *$p \leq 0.05$.

changes of *Vegf3*, *Nodal*, and *Not1* in miR-1 inhibited embryos do not result in a patterning change of PMCs (Fig. 4A and 6). The changes we observed in the spatial expressions of *Vegf3, Nodal, Not1, Bmp2/4,* and *Wnt1* in miR-1 mimic-injected embryos may all contribute to PMC mispatterning (Fig. 4A and 6). Since we did not conduct a time course study to observe changes in gene expression domains, we cannot rule out if these gene expression domain changes are reflective of a developmental delay. However, all control embryos were also injected, so these expression domain changes are not likely due to injections.

Ets1/2, Tbr, and Alx1 are all key regulators of skeletogenesis (Ettensohn et al., 2003; Fuchikami et al., 2002; Oliveri et al., 2008). Of these, we found miR-1 to suppress reporters containing 3′UTRs of *Tbr* and *Ets1/2* (Fig. 5). Tbr plays an essential role in specification of the skeletogenic mesoderm and formation of the larval skeleton where *Tbr* knockdown resulted in a complete loss of skeleton (Oliveri et al., 2002, 2008). Tbr has also been found to be important for PMC EMT, basement membrane remodeling, and apical constriction of PMCs (Saunders and McClay, 2014). We found miR-1 inhibited blastulae have significantly increased *Tbr* mRNA compared to the control (Fig. 7). The impact of *Tbr* overexpression on skeletogenesis in not clear. miR-1's suppression of *Tbr* may potentially contribute to the initial significant delay of PMC ingression (Fig. S1). miR-1 perturbation may also affect *Tbr* levels to impact the level of *msp130*, which is positively activated by Tbr, and encodes one of the biomineralization enzymes (Cary et al., 2017). miR-1 perturbation did not result in significant changes of *Ets1/2* mRNA levels, indicating that miR-1 could regulate *Ets1/2* post-transcriptionally and indirectly by regulating factors that control its function. Ets1, similar to Alx1, provides positive inputs into a large fraction of PMC effector genes (Rafiq et al., 2014). For example, miR-1 perturbation may also affect Ets1 to impact the level of *SM50*, which is activated by Ets1 and encodes one of the biomineralization enzymes (Kurokawa et al., 1999). In general, the effect of inhibition of miR-1 during early blastula/blastula stage, when miR-1 is normally expressed at low level (Fig. 1), on the skeletogenic program may be less consequential than overexpression of miR-1. This may explain the stronger miR-1 overexpression induced skeletal and PMC patterning defects compared to miR-1 inhibition (Figs. 3 and 4).

Interestingly, miR-1 may repress a negative regulator of *Kirrel*, since we observed occasional mispatterned PMCs and shorted tri-radiates in miR-1 inhibited gastrulae (Fig. 4A) (Ettensohn and Dey, 2017). Similarly, miR-1 may repress a negative regulator of *IgTM*, since miR-1 mimic-injected larvae had ectopic skeletal branching, reminiscent of *IgTM* knockdown gastrulae with multiple branching coming out of the tri-radiate rudiment (Figs. 3C and 4B) (Ettensohn and Dey, 2017). Since we did not find miR-1 to directly regulate *IgTM* (Fig. 6B), miR-1's regulation of *IgTM* is likely to be indirect. miR-1 inhibition resulted in significant decrease of *Fgfa* transcript (Fig. 7), indicating that miR-1 likely suppresses a negative regulator of *Fgfa*. Previously it was found that a knockdown of *Fgfa* resulted in PMC mispatterning and a loss of skeleton (Rottinger et al., 2008). This result suggests that decreased *Fgfa* in miR-1 inhibited gastrulae may contribute to the initial shortened tri-radiates but did not impact PMC patterning (Fig. 3A and 4A). Of note is that miRNAs functions by repressing translation of its targets and/or recruiting deadenylase complexes to degrade its target transcript (Lee et al., 1993; Lim et al., 2005; Wightman et al., 1993). Thus, miR-1 may regulate these transcripts at the level of post-transcriptional control and not impacting their transcript levels. Without assaying for their protein levels, we cannot determine how miR-1 regulates these transcripts.

It is interesting to note that miR-1 loss- and gain-of-function lead to similar phenotypes, such as muscle fiber defects (Fig. 2), EMT delay (Fig. S1), and skeletal defects (Fig. 3). We do not know the exact molecular regulatory mechanism of miR-1. However, we propose that such a regulatory mechanism needs to consider the expression of miR-1 (Fig. 1) and miR-1's regulation of multiple targets that impact the same protein or pathway. For example, to explain why miR-1 loss- and gain-of-function lead to similar skeletal defects in the sea urchin, we propose that miR-1 regulates *Ets1/2* and an unidentified negative regulator of Ets1/2. The expression and regulation of Ets1 is complex. The *Ets1* mRNA and protein are maternally present and zygotically expressed during late cleavage stage; its expression is restricted to the skeletogenic lineage until late mesenchyme blastula stage (Kurokawa et al., 1999; Rizzo et al., 2006; Yajima et al., 2010). The function of Ets1 requires phosphorylation ERK for PMC specification (Fernandez-Serra et al., 2004; Rottinger et al., 2004). We propose that miR-1

post-transcriptionally regulates *Ets1/2*, as well as a negative regulator that impacts the function of Ets1/2, such as its phosphatase. The sea urchin genome contains five annotated serine/threonine phosphatases, all of which contain potential miR-1 binding sites. miR-1 is expressed at relatively low levels during early blastula/blastula stages, when Ets1/2 is zygotically expressed and becomes localized to the skeletogenic lineage (Kurokawa et al., 1999; Rizzo et al., 2006; Yajima et al., 2010). Since Ets1/2 is regulated by phosphorylation and becomes functional during the blastula stage, the impact of miR-1 inhibition would result in increased translated Ets1/2 and this unknown negative regulator of Ets1/2. Since the normal expression of miR-1 at the early blastula stage is low, inhibition of miR-1 would not be expected to have a dramatic effect on Ets1/2 and its negative regulator. In this case, phosphorylation of Ets1/2 would result in overall increased functional Ets1, leading to some enhanced expression of PMC effector genes and skeletogenesis. In the case of miR-1 overexpression during the early blastula/blastula stages, when miR-1 is usually at low levels, translation of Ets1/2 and its negative regulator would be decreased. However, the translated Ets1 would be mostly phosphorylated and functional, leading to enhanced PMC effector gene expression and skeletogenesis. Thus, in this proposed mechanism, through miR-1's regulation of *Ets1/2* and its phosphatase, the loss- and gain-of-function of miR-1 would result in similar phenotypes.

An alternative regulatory mechanism could be that miR-1 has variable level of suppression on multiple targets that encode factors that influence muscle, PMC EMT, and skeletogenesis. For example, in the case of skeletogenesis, miR-1's suppression of skeletogenic promoting factors may be less than the level of miR-1's suppression of skeletogenic repressive factors during early blastula/blastula stages. Thus, the net effect would be that miR-1 inhibition is less impactful during a time when its normal expression is low, so that the overall skeletogenic program would not be greatly affected. Upon miR-1 overexpression, the suppression of skeletogenic repressive factors would be greater than the suppression of skeletogenic promoting factors. Thus, during early blastula/blastula stages, excess miR-1 would greatly suppress the skeletogenic repressive factors more than the skeletogenic promoting factors.

We propose that in cases when miR-1 targets a TF or regulator of the skeletogenic program, we would observe reciprocal responses. However, if miR-1 directly targets a TF or regulator of the skeletogenic program as well as a negative regulator of this target during the early blastula/blastula stages, then we would observe similar defects upon either miR-1 inhibition or overexpression. These proposed mechanisms are speculative and will need to be tested in future studies.

Previously, we identified that miR-31 in the sea urchin regulates skeletogenesis by directly suppressing *Eve* and *Wnt1* (Sampilo et al., 2021). Depletion of miR-31 resulted in expanded vegetal spatial expression of *Vegf3* (Sampilo et al., 2021; Stepicheva and Song, 2015), similar to miR-1 mimic injections. Here we identified miR-1 to likely directly suppresses *Ets1/2, Tbr, VegfR7* and *Wnt1,* of which *Ets1/2* and *Tbr* are downstream of miR-31 targets *Pmar1* and *Eve* (Sampilo et al., 2021; Stepicheva and Song, 2015). Thus, both miR-31 and miR-1 target critical components within the PMC GRN and co-regulate skeletogenesis.

5. Conclusions

Overall, we identified miR-1 to be broadly expressed with diverse functions in the sea urchin embryo. miR-1 regulates not only mesodermally-derived gut muscle structures, but also mediate skeletal development. This study identifies novel functions of miR-1, by identifying its likely direct targets and revealing miR-1 to regulate various transcription factors of the PMC GRN and signaling components to regulate skeletogenesis of the developing embryo.

CRediT authorship contribution statement

Nina Faye Sampilo: Data curation, Formal analysis, Investigation, Methodology, Writing – original draft. **Jia L. Song:** Conceptualization, Formal analysis, Funding acquisition, Investigation, Resources, Supervision, Visualization, Writing – review & editing.

Data availability

Data will be made available on request.

Acknowledgements

The authors would like to thank David McClay (Duke University) for his kind gift of 1D5 antibody. We would like to thank Malcolm Arnott for his help on miR-1 F*I*SH. We thank the anonymous Reviewers for their invaluable feedback. This work is funded by University of Delaware Graduate Fellowship to NFS, NSF MCB 2103453 to JLS, NIH NIGMS P20GM103446, and NIH P20GM103653. The usage of the Zeiss LSM 980 multiphoton confocal microscope is funded by NIH grant#1S10RR027273-01.

Appendix A. Supplementary data

Supplementary data to this article can be found online at https://doi.org/10.1016/j.ydbio.2024.01.010.

References

Adomako-Ankomah, A., Ettensohn, C.A., 2011. P58-A and P58-B: novel proteins that mediate skeletogenesis in the sea urchin embryo. Dev. Biol. 353, 81–93.
Adomako-Ankomah, A., Ettensohn, C.A., 2013. Growth factor-mediated mesodermal cell guidance and skeletogenesis during sea urchin gastrulation. Development 140, 4214–4225.
Adonin, L., Drozdov, A., Barlev, N.A., 2020. Sea urchin as a universal model for studies of gene networks. Front. Genet. 11, 627259.
Annunziata, R., Andrikou, C., Perillo, M., Cuomo, C., Arnone, M.I., 2019. Development and evolution of gut structures: from molecules to function. Cell Tissue Res. 377, 445–458.
Annunziata, R., Arnone, M.I., 2014. A dynamic regulatory network explains ParaHox gene control of gut patterning in the sea urchin. Development 141, 2462–2472.
Arenas-Mena, C., Cameron, A.R., Davidson, E.H., 2000. Spatial expression of Hox cluster genes in the ontogeny of a sea urchin. Development 127, 4631–4643.
Arshinoff, B.I., Cary, G.A., Karimi, K., Foley, S., Agalakov, S., Delgado, F., Lotay, V.S., Ku, C.J., Pells, T.J., Beatman, T.R., Kim, E., Cameron, R.A., Vize, P.D., Telmer, C.A., Croce, J.C., Ettensohn, C.A., Hinman, V.F., 2022. Echinobase: leveraging an extant model organism database to build a knowledgebase supporting research on the genomics and biology of echinoderms. Nucleic Acids Res. 50, D970–D979.
Bradham, C.A., Miranda, E.L., McClay, D.R., 2004. PI3K inhibitors block skeletogenesis but not patterning in sea urchin embryos. Dev. Dynam. 229, 713–721.
Cary, G.A., Cheatle Jarvela, A.M., Francolini, R.D., Hinman, V.F., 2017. Genome-wide use of high- and low-affinity Tbrain transcription factor binding sites during echinoderm development. Proc. Natl. Acad. Sci. U.S.A. 114, 5854–5861.
Cheers, M.S., Ettensohn, C.A., 2004. Rapid microinjection of fertilized eggs. Methods Cell Biol. 74, 287–310.
Cheers, M.S., Ettensohn, C.A., 2005. P16 is an essential regulator of skeletogenesis in the sea urchin embryo. Dev. Biol. 283, 384–396.
Chen, J.F., Mandel, E.M., Thomson, J.M., Wu, Q., Callis, T.E., Hammond, S.M., Conlon, F.L., Wang, D.Z., 2006. The role of microRNA-1 and microRNA-133 in skeletal muscle proliferation and differentiation. Nat. Genet. 38, 228–233.
Cole, A.G., Rizzo, F., Martinez, P., Fernandez-Serra, M., Arnone, M.I., 2009. Two ParaHox genes, SpLox and SpCdx, interact to partition the posterior endoderm in the formation of a functional gut. Development 136, 541–549.
Conboy, I.M., Rando, T.A., 2002. The regulation of Notch signaling controls satellite cell activation and cell fate determination in postnatal myogenesis. Dev. Cell 3, 397–409.
Cui, M., Siriwon, N., Li, E., Davidson, E.H., Peter, I.S., 2014. Specific functions of the Wnt signaling system in gene regulatory networks throughout the early sea urchin embryo. Proc. Natl. Acad. Sci. U.S.A. 111, E5029–E5038.
Dal-Pra, S., Furthauer, M., Van-Celst, J., Thisse, B., Thisse, C., 2006. Noggin1 and Follistatin-like2 function redundantly to Chordin to antagonize BMP activity. Dev. Biol. 298, 514–526.
Davidson, E.H., Rast, J.P., Oliveri, P., Ransick, A., Calestani, C., Yuh, C.H., Minokawa, T., Amore, G., Hinman, V., Arenas-Mena, C., Otim, O., Brown, C.T., Livi, C.B., Lee, P.Y., Revilla, R., Rust, A.G., Pan, Z., Schilstra, M.J., Clarke, P.J., Arnone, M.I., Rowen, L., Cameron, R.A., McClay, D.R., Hood, L., Bolouri, H., 2002a. A genomic regulatory network for development. Science 295, 1669–1678.

Davidson, E.H., Rast, J.P., Oliveri, P., Ransick, A., Calestani, C., Yuh, C.H., Minokawa, T., Amore, G., Hinman, V., Arenas-Mena, C., Otim, O., Brown, C.T., Livi, C.B., Lee, P.Y., Revilla, R., Schilstra, M.J., Clarke, P.J., Rust, A.G., Pan, Z., Arnone, M.I., Rowen, L., Cameron, R.A., McClay, D.R., Hood, L., Bolouri, H., 2002b. A provisional regulatory gene network for specification of endomesoderm in the sea urchin embryo. Dev. Biol. 246, 162–190.
Davis, S., Lollo, B., Freier, S., Esau, C., 2006. Improved targeting of miRNA with antisense oligonucleotides. Nucleic Acids Res. 34, 2294–2304.
De Robertis, E.M., 2006. Spemann's organizer and self-regulation in amphibian embryos. Nat. Rev. Mol. Cell Biol. 7, 296–302.
Duboc, V., Lapraz, F., Saudemont, A., Bessodes, N., Mekpoh, F., Haillot, E., Quirin, M., Lepage, T., 2010. Nodal and BMP2/4 pattern the mesoderm and endoderm during development of the sea urchin embryo. Development 137, 223–235.
Duboc, V., Rottinger, E., Besnardeau, L., Lepage, T., 2004. Nodal and BMP2/4 signaling organizes the oral-aboral axis of the sea urchin embryo. Dev. Cell 6, 397–410.
Duloquin, L., Lhomond, G., Gache, C., 2007. Localized VEGF signaling from ectoderm to mesenchyme cells controls morphogenesis of the sea urchin embryo skeleton. Development 134, 2293–2302.
Ettensohn, C.A., Dey, D., 2017. KirrelL, a member of the Ig-domain superfamily of adhesion proteins, is essential for fusion of primary mesenchyme cells in the sea urchin embryo. Dev. Biol. 421, 258–270.
Ettensohn, C.A., Illies, M.R., Oliveri, P., De Jong, D.L., 2003. Alx1, a member of the Cart1/Alx3/Alx4 subfamily of Paired-class homeodomain proteins, is an essential component of the gene network controlling skeletogenic fate specification in the sea urchin embryo. Development 130, 2917–2928.
Ettensohn, C.A., McClay, D.R., 1986. The regulation of primary mesenchyme cell migration in the sea urchin embryo: transplantations of cells and latex beads. Dev. Biol. 117, 380–391.
Fernandez-Serra, M., Consales, C., Livigni, A., Arnone, M.I., 2004. Role of the ERK-mediated signaling pathway in mesenchyme formation and differentiation in the sea urchin embryo. Dev. Biol. 268, 384–402.
Floc'hlay, S., Molina, M.D., Hernandez, C., Haillot, E., Thomas-Chollier, M., Lepage, T., Thieffry, D., 2021. Deciphering and modelling the TGF-beta signalling interplays specifying the dorsal-ventral axis of the sea urchin embryo. Development 148.
Fromm, B., Billipp, T., Peck, L.E., Johansen, M., Tarver, J.E., King, B.L., Newcomb, J.M., Sempere, L.F., Flatmark, K., Hovig, E., Peterson, K.J., 2015. A uniform system for the annotation of vertebrate microRNA genes and the evolution of the human microRNAome. Annu. Rev. Genet. 49, 213–242.
Fuchikami, T., Mitsunaga-Nakatsubo, K., Amemiya, S., Hosomi, T., Watanabe, T., Kurokawa, D., Kataoka, M., Harada, Y., Satoh, N., Kusunoki, S., Takata, K., Shimotori, T., Yamamoto, T., Sakamoto, N., Shimada, H., Akasaka, K., 2002. T-brain homologue (HpTb) is involved in the archenteron induction signals of micromere descendant cells in the sea urchin embryo. Development 129, 5205–5216.
Gildor, T., Winter, M.R., Layous, M., Hijaze, E., Ben-Tabou de-Leon, S., 2021. The biological regulation of sea urchin larval skeletogenesis - from genes to biomineralized tissue. J. Struct. Biol. 213, 107797.
Kadri, S., Hinman, V.F., Benos, P.V., 2011. RNA deep sequencing reveals differential microRNA expression during development of sea urchin and sea star. PLoS One 6, e29217.
Khokha, M.K., Yeh, J., Grammer, T.C., Harland, R.M., 2005. Depletion of three BMP antagonists from Spemann's organizer leads to a catastrophic loss of dorsal structures. Dev. Cell 8, 401–411.
Khor, J.M., Ettensohn, C.A., 2022. Architecture and evolution of the cis-regulatory system of the echinoderm kirrelL gene. Elife 11.
Kiecker, C., Niehrs, C., 2001. A morphogen gradient of Wnt/beta-catenin signalling regulates anteroposterior neural patterning in Xenopus. Development 128, 4189–4201.
Kimura-Yoshida, C., Nakano, H., Okamura, D., Nakao, K., Yonemura, S., Belo, J.A., Aizawa, S., Matsui, Y., Matsuo, I., 2005. Canonical Wnt signaling and its antagonist regulate anterior-posterior axis polarization by guiding cell migration in mouse visceral endoderm. Dev. Cell 9, 639–650.
Konrad, K., Song, J.L., 2022. microRNA-124 regulates Notch and NeuroD1 to mediate transition states of neuronal development. Dev. Neurobiol.
Konrad, K.D., Arnott, M., Testa, M., Suarez, S., Song, J.L., 2023. microRNA-124 directly suppresses Nodal and Notch to regulate mesodermal development. Dev. Biol. 502, 50–62.
Kopan, R., Nye, J.S., Weintraub, H., 1994. The intracellular domain of mouse Notch: a constitutively activated repressor of myogenesis directed at the basic helix-loop-helix region of MyoD. Development 120, 2385–2396.
Kurokawa, D., Kitajima, T., Mitsunaga-Nakatsubo, K., Amemiya, S., Shimada, H., Akasaka, K., 1999. HpEts, an ets-related transcription factor implicated in primary mesenchyme cell differentiation in the sea urchin embryo. Mech. Dev. 80, 41–52.
Lapraz, F., Besnardeau, L., Lepage, T., 2009. Patterning of the dorsal-ventral axis in echinoderms: insights into the evolution of the BMP-chordin signaling network. PLoS Biol. 7, e1000248.
Layous, M., Khalaily, L., Gildor, T., Ben-Tabou de-Leon, S., 2021. The tolerance to hypoxia is defined by a time-sensitive response of the gene regulatory network in sea urchin embryos. Development 148.
Leaf, D.S., Anstrom, J.A., Chin, J.E., Harkey, M.A., Showman, R.M., Raff, R.A., 1987. Antibodies to a fusion protein identify a cDNA clone encoding msp130, a primary mesenchyme-specific cell surface protein of the sea urchin embryo. Dev. Biol. 121, 29–40.
Lee, R.C., Feinbaum, R.L., Ambros, V., 1993. The C. elegans heterochronic gene lin-4 encodes small RNAs with antisense complementarity to lin-14. Cell 75, 843–854.
Li, E., Cui, M., Peter, I.S., Davidson, E.H., 2014. Encoding regulatory state boundaries in the pregastrular oral ectoderm of the sea urchin embryo. Proc. Natl. Acad. Sci. U.S.A. 111, E906–E913.
Li, E., Materna, S.C., Davidson, E.H., 2012. Direct and indirect control of oral ectoderm regulatory gene expression by Nodal signaling in the sea urchin embryo. Dev. Biol. 369, 377–385.
Lim, L.P., Lau, N.C., Garrett-Engele, P., Grimson, A., Schelter, J.M., Castle, J., Bartel, D. P., Linsley, P.S., Johnson, J.M., 2005. Microarray analysis shows that some microRNAs downregulate large numbers of target mRNAs. Nature 433, 769–773.
Liu, C., Wang, J., Zhang, X., 2014. The involvement of MiR-1-clathrin pathway in the regulation of phagocytosis. PLoS One 9, e98747.
Livingston, B.T., Killian, C.E., Wilt, F., Cameron, A., Landrum, M.J., Ermolaeva, O., Sapojnikov, V., Maglott, D.R., Buchanan, A.M., Ettensohn, C.A., 2006. A genome-wide analysis of biomineralization-related proteins in the sea urchin Strongylocentrotus purpuratus. Dev. Biol. 300, 335–348.
Logan, C.Y., Miller, J.R., Ferkowicz, M.J., McClay, D.R., 1999. Nuclear beta-catenin is required to specify vegetal cell fates in the sea urchin embryo. Development 126, 345–357.
Mansfield, J.H., Harfe, B.D., Nissen, R., Obenauer, J., Srineel, J., Chaudhuri, A., Farzan-Kashani, R., Zuker, M., Pasquinelli, A.E., Ruvkun, G., Sharp, P.A., Tabin, C.J., McManus, M.T., 2004. MicroRNA-responsive 'sensor' transgenes uncover Hox-like and other developmentally regulated patterns of vertebrate microRNA expression. Nat. Genet. 36, 1079–1083.
Materna, S.C., Ransick, A., Li, E., Davidson, E.H., 2013. Diversification of oral and aboral mesodermal regulatory states in pregastrular sea urchin embryos. Dev. Biol. 375, 92–104.
McCarthy, J.J., 2011. The MyomiR network in skeletal muscle plasticity. Exerc. Sport Sci. Rev. 39, 150–154.
McClay, D.R., Cannon, G.W., Wessel, G.M., Fink, R.D., Marchase, R.B., 1983. Time, Space, and Pattern in Embryonic Development.
Mishima, Y., Stahlhut, C., Giraldez, A.J., 2007. miR-1-2 gets to the heart of the matter. Cell 129, 247–249.
Morgulis, M., Gildor, T., Roopin, M., Sher, N., Malik, A., Lalzar, M., Dines, M., Ben-Tabou de-Leon, S., Khalaily, L., Ben-Tabou de-Leon, S., 2019. Possible cooption of a VEGF-driven tubulogenesis program for biomineralization in echinoderms. Proc. Natl. Acad. Sci. U.S.A. 116, 12353–12362.
Morgulis, M., Winter, M.R., Shternhell, L., Gildor, T., Ben-Tabou de-Leon, S., 2021. VEGF signaling activates the matrix metalloproteinases, MmpL7 and MmpL5 at the sites of active skeletal growth and MmpL7 regulates skeletal elongation. Dev. Biol. 473, 80–89.
Nguyen, H.T., Frasch, M., 2006. MicroRNAs in muscle differentiation: lessons from Drosophila and beyond. Curr. Opin. Genet. Dev. 16, 533–539.
Oliveri, P., Carrick, D.M., Davidson, E.H., 2002. A regulatory gene network that directs micromere specification in the sea urchin embryo. Dev. Biol. 246, 209–228.
Oliveri, P., Tu, Q., Davidson, E.H., 2008. Global regulatory logic for specification of an embryonic cell lineage. Proc. Natl. Acad. Sci. U.S.A. 105, 5955–5962.
Orom, U.A., Kauppinen, S., Lund, A.H., 2006. LNA-modified oligonucleotides mediate specific inhibition of microRNA function. Gene 372, 137–141.
Owczarzy, R., You, Y., Groth, C.L., Tataurov, A.V., 2011. Stability and mismatch discrimination of locked nucleic acid-DNA duplexes. Biochemistry 50, 9352–9367.
Peng, W., Yu, S., Handler, A.M., Tu, Z., Saccone, G., Xi, Z., Zhang, H., 2020. miRNA-1-3p is an early embryonic male sex-determining factor in the Oriental fruit fly Bactrocera dorsalis. Nat. Commun. 11, 932.
Qiagen, 2018. RNA Functional Analysis - Enhanced by LNA.
Rafiq, K., Shashikant, T., McManus, C.J., Ettensohn, C.A., 2014. Genome-wide analysis of the skeletogenic gene regulatory network of sea urchins. Development 141, 950–961.
Range, R.C., Wei, Z., 2016. An anterior signaling center patterns and sizes the anterior neuroectoderm of the sea urchin embryo. Development 143, 1523–1533.
Remsburg, C., Konrad, K., Sampilo, N.F., Song, J.L., 2019. Analysis of microRNA functions. Methods Cell Biol. 151, 323–334.
Revilla-i-Domingo, R., Oliveri, P., Davidson, E.H., 2007. A missing link in the sea urchin embryo gene regulatory network: hesC and the double-negative specification of micromeres. Proc. Natl. Acad. Sci. U.S.A. 104, 12383–12388.
Rizzo, F., Fernandez-Serra, M., Squarzoni, P., Archimandritis, A., Arnone, M.I., 2006. Identification and developmental expression of the ets gene family in the sea urchin (Strongylocentrotus purpuratus). Dev. Biol. 300, 35–48.
Roberts, P., Noerholm, M., Ståhlberg, N., Mouritzen, P., Glue, C., 2006. miRCURY™ LNA research tools for microRNA. Nat. Methods 3, I–II.
Rottinger, E., Besnardeau, L., Lepage, T., 2004. A Raf/MEK/ERK signaling pathway is required for development of the sea urchin embryo micromere lineage through phosphorylation of the transcription factor Ets. Development 131, 1075–1087.
Rottinger, E., Saudemont, A., Duboc, V., Besnardeau, L., McClay, D., Lepage, T., 2008. FGF signals guide migration of mesenchymal cells, control skeletal morphogenesis [corrected] and regulate gastrulation during sea urchin development. Development 135, 353–365.
Rozen, S., Skaletsky, H., 2000. Primer3 on the WWW for general users and for biologist programmers. Methods Mol. Biol. 132, 365–386.
Sampilo, N.F., Stepicheva, N.A., Song, J.L., 2021. microRNA-31 regulates skeletogenesis by direct suppression of Eve and Wnt1. Dev. Biol. 472, 98–114.
Sampilo, N.F., Stepicheva, N.A., Zaidi, S.A.M., Wang, L., Wu, W., Wikramanayake, A., Song, J.L., 2018. Inhibition of microRNA suppression of Dishevelled results in Wnt pathway-associated developmental defects in sea urchin. Development 145.
Saudemont, A., Haillot, E., Mekpoh, F., Bessodes, N., Quirin, M., Lapraz, F., Duboc, V., Rottinger, E., Range, R., Oisel, A., Besnardeau, L., Wincker, P., Lepage, T., 2010. Ancestral regulatory circuits governing ectoderm patterning downstream of Nodal

and BMP2/4 revealed by gene regulatory network analysis in an echinoderm. PLoS Genet. 6, e1001259.
Saunders, L.R., McClay, D.R., 2014. Sub-circuits of a gene regulatory network control a developmental epithelial-mesenchymal transition. Development 141, 1503–1513.
Schuster-Gossler, K., Cordes, R., Gossler, A., 2007. Premature myogenic differentiation and depletion of progenitor cells cause severe muscle hypotrophy in Delta1 mutants. Proc. Natl. Acad. Sci. U.S.A. 104, 537–542.
Sepúlveda-Ramírez, S.P., Toledo-Jacobo, L., Henson, J.H., Shuster, C.B., 2018. Cdc42 controls primary mesenchyme cell morphogenesis in the sea urchin embryo. Dev. Biol. 437, 140–151.
Sethi, A.J., Angerer, R.C., Angerer, L.M., 2014. Multicolor labeling in developmental gene regulatory network analysis. Methods Mol. Biol. 1128, 249–262.
Sherwood, D.R., McClay, D.R., 1999. LvNotch signaling mediates secondary mesenchyme specification in the sea urchin embryo. Development 126, 1703–1713.
Sherwood, D.R., McClay, D.R., 2001. LvNotch signaling plays a dual role in regulating the position of the ectoderm-endoderm boundary in the sea urchin embryo. Development 128, 2221–2232.
Simon, D.J., Madison, J.M., Conery, A.L., Thompson-Peer, K.L., Soskis, M., Ruvkun, G.B., Kaplan, J.M., Kim, J.K., 2008. The microRNA miR-1 regulates a MEF-2-dependent retrograde signal at neuromuscular junctions. Cell 133, 903–915.
Sokol, N.S., Ambros, V., 2005. Mesodermally expressed Drosophila microRNA-1 is regulated by Twist and is required in muscles during larval growth. Genes Dev. 19, 2343–2354.
Song, J.L., Stoeckius, M., Maaskola, J., Friedlander, M., Stepicheva, N., Juliano, C., Lebedeva, S., Thompson, W., Rajewsky, N., Wessel, G.M., 2011. Select microRNAs are essential for early development in the sea urchin. Developmental Biology.
Stahlhut, C., Suarez, Y., Lu, J., Mishima, Y., Giraldez, A.J., 2012. miR-1 and miR-206 regulate angiogenesis by modulating VegfA expression in zebrafish. Development 139, 4356–4364.
Staton, A.A., Giraldez, A.J., 2011. Use of target protector morpholinos to analyze the physiological roles of specific miRNA-mRNA pairs in vivo. Nat. Protoc. 6, 2035–2049.
Stepicheva, N., Nigam, P.A., Siddam, A.D., Peng, C.F., Song, J.L., 2015. microRNAs regulate beta-catenin of the Wnt signaling pathway in early sea urchin development. Dev. Biol. 402, 127–141.
Stepicheva, N.A., Song, J.L., 2014. High throughput microinjections of sea urchin zygotes. J. Vis. Exp., e50841
Stepicheva, N.A., Song, J.L., 2015. microRNA-31 modulates skeletal patterning in the sea urchin embryo. Development 142, 3769–3780.
Sweet, H.C., Gehring, M., Ettensohn, C.A., 2002. LvDelta is a mesoderm-inducing signal in the sea urchin embryo and can endow blastomeres with organizer-like properties. Development 129, 1945–1955.
Takemura, M., Bowden, N., Lu, Y.S., Nakato, E., O'Connor, M.B., Nakato, H., 2021. Drosophila MOV10 regulates the termination of midgut regeneration. Genetics 218.
Walton, K.D., Warner, J., Hertzler, P.H., McClay, D.R., 2009. Hedgehog signaling patterns mesoderm in the sea urchin. Dev. Biol. 331, 26–37.
Wei, Z., Yaguchi, J., Yaguchi, S., Angerer, R.C., Angerer, L.M., 2009. The sea urchin animal pole domain is a Six3-dependent neurogenic patterning center. Development 136, 1179–1189.
Wheeler, B.M., Heimberg, A.M., Moy, V.N., Sperling, E.A., Holstein, T.W., Heber, S., Peterson, K.J., 2009. The deep evolution of metazoan microRNAs. Evol. Dev. 11, 50–68.
Wienholds, E., Kloosterman, W.P., Miska, E., Alvarez-Saavedra, E., Berezikov, E., de Bruijn, E., Horvitz, H.R., Kauppinen, S., Plasterk, R.H., 2005. MicroRNA expression in zebrafish embryonic development. Science 309, 310–311.
Wightman, B., Ha, I., Ruvkun, G., 1993. Posttranscriptional regulation of the heterochronic gene lin-14 by lin-4 mediates temporal pattern formation in C. elegans. Cell 75, 855–862.
Wikramanayake, A.H., Huang, L., Klein, W.H., 1998. beta-Catenin is essential for patterning the maternally specified animal-vegetal axis in the sea urchin embryo. Proc. Natl. Acad. Sci. U.S.A. 95, 9343–9348.
Winter, M.R., Morgulis, M., Gildor, T., Cohen, A.R., Ben-Tabou de-Leon, S., 2021. Calcium-vesicles perform active diffusion in the sea urchin embryo during larval biomineralization. PLoS Comput. Biol. 17, e1008780.
Xu, P.F., Houssin, N., Ferri-Lagneau, K.F., Thisse, B., Thisse, C., 2014. Construction of a vertebrate embryo from two opposing morphogen gradients. Science 344, 87–89.
Yajima, M., Umeda, R., Fuchikami, T., Kataoka, M., Sakamoto, N., Yamamoto, T., Akasaka, K., 2010. Implication of HpEts in gene regulatory networks responsible for specification of sea urchin skeletogenic primary mesenchyme cells. Zool. Sci. (Tokyo) 27, 638–646.
Yuh, C.H., Brown, C.T., Livi, C.B., Rowen, L., Clarke, P.J., Davidson, E.H., 2002. Patchy interspecific sequence similarities efficiently identify positive cis-regulatory elements in the sea urchin. Dev. Biol. 246, 148–161.
Zhao, Y., Ransom, J.F., Li, A., Vedantham, V., von Drehle, M., Muth, A.N., Tsuchihashi, T., McManus, M.T., Schwartz, R.J., Srivastava, D., 2007. Dysregulation of cardiogenesis, cardiac conduction, and cell cycle in mice lacking miRNA-1-2. Cell 129, 303–317.
Zhao, Y., Samal, E., Srivastava, D., 2005. Serum response factor regulates a muscle-specific microRNA that targets Hand2 during cardiogenesis. Nature 436, 214–220.